Aalto University
School of Chemical
Engineering

Konrad Klockars

Evaporation-induced self-assembly of cellulose nanocrystals from aqueous suspensions into chiral nematic solid structures

Master's Programme in Chemical, Biochemical and Materials Engineering
Major in Fiber and Polymer Engineering

Master's thesis for the degree of Master of Science in Technology submitted for inspection, Espoo, 13th May 2018.

Supervisor	**Professor Orlando J. Rojas**
Instructors	**Dr. Blaise Tardy**
	Dr. Maryam Borghei

Aalto University
School of Chemical
Engineering

Aalto University, P.O. BOX 11000, 00076 AALTO
www.aalto.fi

Abstract of master's thesis

Author Konrad Klockars		
Title of thesis Evaporation-induced self-assembly of cellulose nanocrystals from aqueous suspensions into chiral nematic solid structures		
Degree program Chemical, Biochamical and Materials Engineering		
Major Fiber and Polymer Engineering		**Major code** CHEM3024
Thesis supervisor Professor Orlando Rojas		
Thesis advisors / Thesis examiners Drs. Blaise Tardy and Maryam Borghei		
Date 13.05.2018	**Number of pages** 67	**Language** English

Abstract

Biobased and renewable cellulose nanocrystals (CNC) can form hierarchically structured assemblies with impressive optical and mechanical properties. These rod-shaped nanoparticles, produced through acid hydrolysis of biomass, self-assemble in aqueous suspensions and form a liquid crystalline anisotropic volume fraction (AVF), the extent of which depends on the concentration. The anisotropic chiral nematic liquid crystalline phase can be preserved in the dry state through evaporation-induced self-assembly (EISA). This transition is not fully understood and requires more thorough inspection, in order to create large-scale defect-free structures for demanding applications, such as impact resistant materials. This work addresses this by studying the conditions during EISA for producing highly ordered CNC films. Solid CNC films display structural colour, whose intensity and uniformity reveal how well the chiral nematic order is preserved and defined within the film. UV-Vis spectroscopy, optical microscopy and scanning electron microscopy (SEM) provide information on the formation and distribution of the structural colour.

In the first part of this work, the EISA drying temperature was varied (23, 28, 36, 41, 51 and 61°C). The results showed deteriorated helical order within solid films produced at higher drying temperatures. This conclusion was deduced from UV-Vis spectroscopy data that implied a larger distribution of structural colours in the films dried at elevated temperatures.

In the second part, five different concentrations of the suspensions (3-7% w/w), and thereby AVFs, were used, while keeping the drying conditions the same. One set of samples was dried immediately after casting, while another set was equilibrated prior to drying. The characterization of the dry films by microscopy, UV-Vis and SEM showed that suspensions dried from a high AVF and an equilibrated state produced films with more homogeneous, long-range order, having larger chiral nematic domains. In contrast, films dried from AVF=0 lacked long-range order and did not benefit from equilibration.

Keywords Cellulose nanocrystals, anisotropic volume fraction, evaporation-induced self-assembly, chiral nematic domain, structural colour

Aalto University
School of Chemical
Engineering

Aalto University, P.O. BOX 11000, 00076 AALTO
www.aalto.fi

Abstract of master's thesis

Författare Konrad Klockars

Titel Avdusntningsinducerad självhopsättning av cellulosananokristaller i vätskesuspensioner till kolesteriska fasta structurer

Studieprogram Kemi-, Biokemi- och Materialteknologi

Huvudämne Fiber- och Polymerteknologi **kod** CHEM3024

Övervakare Professor Orlando Rojas

Handledare Dr. Blaise Tardy, Dr. Maryam Borghei

Datum 13.05.2018 **Sidantal** 67 **Språk** Engelska

Sammanfattning

Biobaserade och förnybara cellulosananokristaller (CNC) kan bilda hierarkiskt strukturerade enheter med imponerande optiska och mekaniska egenskaper. Dessa stavformade nanopartiklar, som produceras genom syrahydrolys av biomassa, självhopsätter sig vätskesuspensioner och bildar en vätksekristallin anisotrop volymfraktion (AVF), vars storlek beror på koncentrationen. Den anisotropa kirala nematiska vätskekristallina fasen bevaras i fast form genom Avdusntningsinducerad självhopsättning (EISA). Denna övergång är inte fullständigt förstådd och kräver noggrannare inspektion för att man skall kunna skapa defektfria strukturer i större skala, för mer krävande tillämpningar, såsom slagfasta material. Detta arbete fokuserar på denna övergång genom att studera omständigheterna under EISA för att producera CNC filmer med en organiserad struktur. Torra CNC filmer uppvisar strukturell färg, vars intensitet och likformighet avslöjar hur väl den chirala nematiska ordningen är bevarad och organiserad. UV-Vis-spektroskopi, optisk mikroskopi och skanningselektronmikroskopi (SEM) avslöjar distributionen av den strukturella färgen.

I den första delen av detta arbete varierades torkningstemperaturen (23, 28, 36, 41, 51 och 61 ° C) under EISA. Enligt resultaten var organiseringen av den önskvärda spriralstrukturen sämre i fasta filmer framställda vid högre torkningstemperaturer. Denna slutsats härleddes från UV-Vis-spektroskopi-data som vars data avslöjade en större fördelning av strukturella färger i filmer producerade i förhöjda temperaturer.

I andra delen användes fem olika suspensionkoncentrationer (3–7% vikt/vikt) och därigenom AVF:er, medan torkningsomständigheterna var konstanta. En uppsättning prover torkades omedelbart efter placeringen i substratet, medan en annan sats jämviktades före torkningen. Karaktäriseringen av torrfilmerna med mikroskopi, UV-Vis och SEM visade att de suspensionerna torkade från en högre AVF och ett jämviktat tillstånd producerade filmer med en mer homogen långdistansordning och större kirala nematiska domäner. Filmer torkade från AVF = 0 och utan jämviktning saknade långdistansordning.

Nyckelord Cellulose nanocrystals, anisotropic volume fraction, evaporation-induced self-assembly, chiral nematic domain, structural colour

ACKNOWLEDGEMENTS

This Master's Thesis was conducted in the Department of Bioproducts and Biosystems at Aalto University's School of Chemical Engineering in Otaniemi, Espoo.

I wish to express my sincere gratitude to Professor Orlando J. Rojas for his trust and confidence in this thesis work. I would like to thank my instructor, Dr. Blaise Tardy, for his extensive guidance through the whole process, which enabled a deeper understanding of the topic. I also express my thanks to my second instructor, Dr. Maryam Borghei, for her encouragement and optimism. I want to thank Marja Kärkkäinen for producing the starting material, and Valeria Azovskaya for taking wonderful photographs of the samples. I feel grateful for being part of the cheerful and inspiring BiCMat research group.

Part of the work performed to realize this master's thesis was used for writing a manuscript that was submitted to the journal Biomacromolecules, where Konrad Klockars was the first author.

Espoo, 13th of May 2018.
Konrad Klockars

CONTENTS

ABBREVIATIONS

AVF	Anisotropic volume fraction
CNC/CNCs	Cellulose nanocrystal/s
CD	Circular dichromism
EISA	Evaporation-induced self-assembly
PEG	Poly(ethylene glycol)
PVA	Poly(vinyl alcohol)
SEM	Scanning electron microscopy
VASA	Vacuum-assisted self-assembly
w	The weight fraction of CNCs in an aqueous suspension
w_0	The critical concentration (weight fraction of CNCs) for self-assembly in solution, $\phi = 0$
w_1	$\phi = 1$
w_k	The concentration (weight fraction of CNCs) for kinetic arrest
ε_r	The relative electric permittivity
ϕ	The AVF on a scale from 0 to 1

FIGURES

TABLES

1. INTRODUCTION

In recent years, there has been a growing interest on nanomaterials derived from renewable resources. Cellulose nanocrystals (CNCs), obtained by top-down processing of plant-based resources, possess suitable properties for novel hierarchically structured materials with outstanding photonic and mechanical properties.[1] These nanosized and rod-shaped particles have potential applications ranging from tissue engineering and drug delivery[2] to solar cells.[3] However, the large-scale production and utilization of CNCs has been hindered by challenges related to the inherent heterogeneity biological materials. This century has seen a great rise in scientific interest for the formation of hierarchically structured materials for CNCs resulting in a significant increase in publications in the field of photonic applications of CNCs.

CNCs are rigid, rod-shaped particles consisting of parallel cellulose chains, with sub-micron sizes that depend on the starting material. They form stable aqueous suspension due to electrostatic stabilization from negatively charged sulphate surface groups. Above a critical concentration, a chiral nematic liquid crystalline phase forms.[4] Solvent casting turns the translucent suspension into solid, helically ordered materials, which display iridescent structural colour.[5-11] Chiral nematic structures are found in animals and plants,[12] providing both colour and strength.

The properties and colour of the dried film are a function of both the equilibrium state of the CNC suspension prior to drying and the complex dynamic phenomena occurring during drying. There have been several attempts to control the colour in the films, by altering both the equilibrium state[13-15] and drying conditions.[5,7,16,17] Although pure CNC films with fully uniform colour have not been made yet, CNC has been used as a template to produce solid silica films with very homogeneous colours.[18]

In addition to their optical properties, cellulose based nanomaterials possess other valuable properties needed in functional materials, such as a high stiffness, low density and a low thermal expansion coefficient. The most immediate applications include security papers,[19] sensors,[20] mirrorless lasing[21] and pigments.[22] However, cellulose nanocrystal films and related materials are very brittle. Plasticizers, such as poly(vinyl alcohol) (PVA),[23] poly(ethylene glycol) (PEG),[24,25] and surfactants[26] have been used to make the films more flexible, while retaining their

iridescence. Unfortunately, additives always reduce the quality of the colour and the optical properties.

Despite the great interest in this topic, the phenomena are still poorly understood that govern the self-assembly and transformation from liquid crystal suspensions into solid iridescent photonic crystals. The science that governs the formation of the solid coloured structures needs to be understood in depth, in order to apply this material as a selective reflector for advanced optics, and also in order to utilize renewable and non-polluting materials as colours in day-to-day applications. This thesis attempts to uncover part of the underlying phenomena, by performing two simple studies. First, establishing a cause-effect relationship between concentration and the equilibrium state of the CNC suspension on the long-range order of the hierarchical structures in the dried films. Second, the dynamic phenomena during drying are studied by changing the drying temperature. Understanding the effect of these two aspects would pave the way for using the material, for instance, in design applications.

2. LITERATURE REVIEW

2.1. Cellulose nanocrystals

Cellulose nanocrystals are crystalline segments of the cellulose microfibril, which is an elementary component in lignocellulose, i.e. plant biomass. The nanocrystals are usually hydrolysed from cellulose rich lignocellulosic materials, such as wood dissolving pulp or cotton filter paper.[27] After mechanical pre-treatment, the fibres are immersed in strong acid, usually 64% sulphuric acid.[28] The amorphous parts of the microfibrils are hydrolysed and the crystalline part is preserved, i.e. the nanocrystals. In Figure 1, the CNCs correspond to the "elementary fibril", after removal of its amorphous regions. The benefit of using sulphuric acid is the installation of charged sulphate groups on the surfaces of the cellulose crystals.[4,29] The sulphate groups provide negative surface charges, which electrostatically stabilize aqueous colloidal suspensions of CNC.[30]

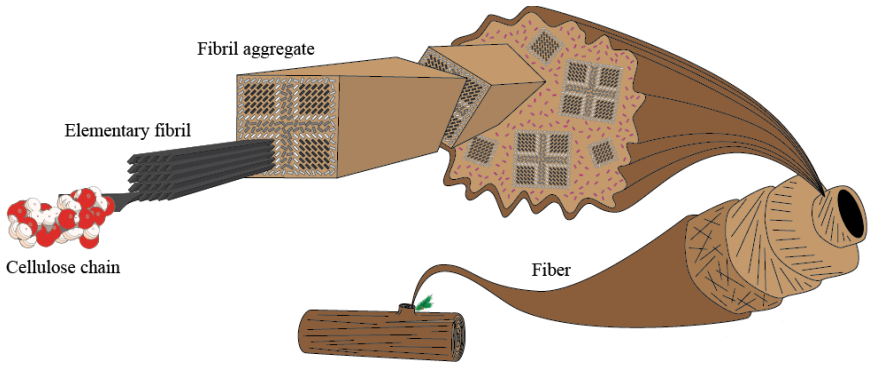

Figure 1. The structure of the elementary components within wood. The "elementary fibril" is the component from the figure that is relevant in this study. After hydrolysis of the "fibre", the crystalline parts of the "elementary fibrils" remain, which are commonly known as cellulose nanocrystals.[31]

2.2. Structural colour

Most materials' colours arise from the pigments they contain. The chemical composition of the pigment determines which light wavelengths are absorbed or reflected. Structural colour, on the other hand, arises from selective light reflection created by the long-range structure within the material, independent of its chemical composition. The elementary components are

themselves transparent, but by organizing into structures in the scale of few hundred nanometres, the materials display colours across the whole visible wavelength spectrum. These structures can also reflect infrared or UV-light. They are found in nature in both plants and animals,[12,32] where they function both as colour producing and mechanical reinforcement structures. Several efforts have been made to biomimic these structures to produce mechanically strong composite materials.[33] A common way to by which nature organizes the structures is by stacking layers of fibrillar or rod-like elementary components, where they are oriented in each layer are oriented in a certain direction and the orientation is slightly shifted to one direction in each subsequent layer. This creates a helicoidal structure[33] that functions as a photonic crystal,[34] which selectively reflects circularly polarized light with the same direction or handedness as the helicoid.[35]

2.3. Cellulose nanocrystals form chiral nematic liquid crystals and structural colour in solid materials

Cellulose nanocrystals self-assemble into chiral nematic, also called cholesteric, liquid crystal phases in liquid suspensions when the concentration of CNC (w/w), is above a critical concentration, w_0.[4,36] Increasing the concentration of nanocrystals increases the fraction of crystals that form the chiral nematic phase, i.e. the anisotropic volume fraction (AVF). In Figure 2b, the lighter part of the suspension in the vial corresponds to the AVF (Figure 2a), whereas the dark part corresponds to the isotropic volume fraction (Figure 2c).

The chiral nematic liquid crystalline structure consists of layers of nematic nanocrystals, called chiral nematic pseudo-phases or pseudo-layers, stacked on top of each other, where the crystals in each layer are oriented along a common director (Figure 2a). The director, which is always orthogonal to the chiral nematic axis, is then modulated helically along an axis. The direction of the modulation can be either right- or left-handed. The distance along the chiral nematic axis where the director has rotated 360° is defined as the pitch length. The double arrow in Figure 2a indicates the half pitch size, corresponding to a 180° rotation. Nanocrystals always have a left-handed arrangement in this twisted planar structure, which selectively reflects left-handed circularly polarized light, and transmits right-handed polarized light.[37-39]

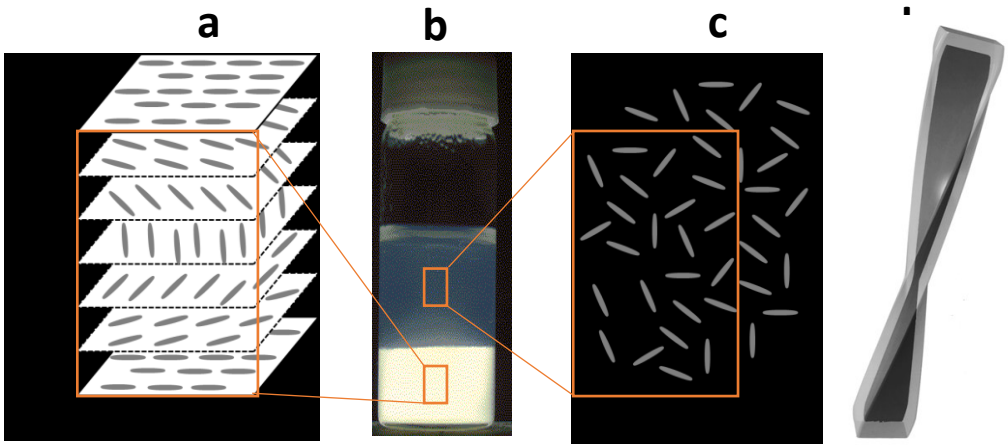

Figure 2. (a) Schematic of the chiral nematic liquid crystalline phase within the anisotropic volume fraction. The CNCs are organized in layers stacked upon each other, where the CNCs within one layer are oriented in the same direction, and the orientation in each subsequent layer is slightly modulated along the vertical chiral nematic axis (double arrow), to produce a helix. (b) A CNC suspension after phase separation. The vial is placed between crossed polarizers, with a light source at one end and the camera at the other. The AVF appears bright because circularly polarized light, which may pass through the polarizer, is reflected from the chiral nematic liquid crystalline structuring. (c) The schematic shows that CNCs lack long-range organization within the isotropic volume fraction. (d) Schematic of a single cellulose nanocrystal, showing its inherent twist along its axis.[40,41]

The time-dependent self-assembly of the nanocrystals depends on their isolation method. The very stable nanocrystals made using sulphuric acid hydrolysis[4] attain an equilibrium state after a few weeks, while CNC hydrolysed with another acid, e.g. hydrochloric acid, may attain an equilibrium only after months, or possibly never.[42]

Onsager[43] proposed a model to predict the behaviour of colloidal particles in a volume of liquid. The formation of ordered structures, i.e. liquid crystals in the case of cellulose nanocrystals, depends on the aspect ratio of the nanorods. The model considers the effective volume of the particles, which is extended by electrostatic repulsions. The partial phase transition into nematic or chiral nematic phases requires lower volume fractions of rods when their aspect ratio is higher, i.e. the onset of phase separation occurs at lower concentrations for longer and thinner rods. Above the critical concentration, it is more favourable for some of the nanorods to exist in a nematic arrangement, due to an increase in free volume and packing entropy for the nematically oriented nanorod fraction.

CNCs are rigid, rod-shaped particles, but they are not fully straight. They are slightly twisted along their long axis, as shown in Figure 2d.[44] It is this inherent right-handed twist that causes the packing into a left-handed chiral nematic, instead of nematic, assemblies. The CNCs pack more effectively and reduce the total volume if they are packed in a helical, chiral nematic arrangement. This twist extends to the effective volume of the CNC, but it is screened at large electrostatic double layers (at high surface charge). Therefore, the CNCs can pack tighter when salt is added to screen the surface charges and reduce the effective volume.[39,40] Although Marchessault et al.[45] observed liquid crystalline textures in a nanocrystal suspension derived from cellulosic material through acid hydrolysis, Revol et al.[4] were the first to discover that they self-assemble into helical chiral nematic structures at a critical concentration, as predicted earlier by the Onsager theory for charged nanorods.

Fingerprint areas can be observed in chiral nematic CNC suspensions with polarized optical microscopy (POM), where the distance between the black bands correspond to half the pitch value. This is only possible when the chiral nematic axis is perfectly perpendicular to the direction of observation. The pitch in the suspension is usually in the micrometric range.[4,46]

This chiral nematic ordering can be preserved in the solid state. By allowing the liquid, which is usually water, to evaporate, a dried film can be obtained, where the pitch is reduced to hundreds of nanometres. This method is called evaporation induced self-assembly (EISA). [5,6,14] Other methods exist to preserve the chiral nematic ordering in solid CNC films, e.g. vacuum assisted self-assembly (VASA).[47]

De Vries[35] correlated the pitch with the circularly polarized reflected light of a chiral nematic liquid crystal, according to the Braggs law - Equation 1 - below, where p corresponds to the pitch, n to the average value of the refractive index of the film, and θ the angle of incidence. This angle refers to the angle between the vector of the incoming light and the chiral nematic axis (double arrow in Figure 2a).

$$\text{Equation 1: } \lambda = n * \frac{P}{2} * \cos(\theta)$$

The refractive index depends on the liquid crystal molecular structure, composition and orientation. Dried films act as photonic films that give rise to iridescent structural colour, due to

thin-film interference and, principally, Bragg reflection of light in the visible range.[34,48,49] The left-handed helically ordered structure will selectively reflect left-handed circularly polarized light and transmit right-handed polarized light.[35]

2.4. Factors affecting the anisotropic volume fraction and pitch in cellulose nanocrystal suspensions

Several factors determine the pitch and the anisotropic volume fraction, such as the CNC concentration, CNC dimensions, surface charge and solvent. This section discusses the effect of these conditions on the equilibrium state of cellulose nanocrystals in water suspensions, whereas section 2.5. describes the non-equilibrium conditions and their effects during and after EISA.

2.4.1. Suspension concentration

Suspensions of cellulose nanocrystals with a low volumetric concentration consist of a single isotropic phase, where the nanocrystals are oriented in random directions. Above a critical concentration (w_0) a fraction of the nanocrystals will form an anisotropic chiral nematic phase.[36] ϕ is commonly used to indicate the chiral nematic volume fraction in CNC suspensions. As the concentration increases, ϕ also increases. At a certain concentration, w_1, ϕ equals one. The values for w_0 and w_1 highly depend on the inherent nanocrystal properties[29], as is discussed in section 2.4.2. As an example, Honorato-Rios et al.[13] observed that > 11 wt% concentration of CNC was required for ϕ=1 (w_1), in the case of their cotton-based CNCs produced with sulphuric acid.

The nanocrystals in the chiral nematic phase are more tightly packed than in the isotropic phase, making the chiral nematic phase denser. Over time, tactoids with chiral nematic order will form a lower anisotropic volume fraction in a container.[36] This can be observed by POM, through crossed polarizers, and the anisotropic volume fraction can be calculated from the relative volumes of the bright chiral nematic phase and the plain isotropic phase. Dong et al.[29] observed a concentration difference between the two phases, the lower anisotropic phase being more concentrated. The concentration also affects the pitch value in the anisotropic phase with the pitch decreasing with increasing concentration.[4,13] In addition to the isotropic and

anisotropic phase, Honorato-Rios et al.[13] observed an intermediate phase that might host CNCs constantly shifting between a liquid crystalline and a non-liquid crystalline phase.

2.4.2. Inherent cellulose nanocrystal properties

Chiral nematic phase formation require specific CNC characteristics, such as surface charge and aspect ratio, which can be altered by changing the biomass source and hydrolysis conditions. CNCs produced through sulphuric acid hydrolysis only form chiral nematic phases when hydrolysed within a certain temperature and time range.[29,46] However, it is worth noting that these ranges depend on the cellulose source. Longer reaction times and higher temperatures during the hydrolysis produce shorter nanocrystals with higher surface charge. Furthermore, the size distribution also becomes narrower.[50]

Beck-Candadedo et al.[46] found that shorter CNCs with lower aspect ratios and larger surface charge have higher w_0 values. Abitbol et al.[51] compared CNCs of similar size but different charge, and concluded that w_0 increased only as an effect of increasing charge. When the particles are too large, they tend to aggregate and gel before w_0, which effectively hinders the self-assembly into liquid crystals. In polydisperse suspensions, a longer fraction has been observed in the anisotropic phase and a shorter fraction have been observed in the isotropic phase, for both CNCs[29] and bacterial cellulose.[52] The particle properties also affects the pitch in suspension. Increased nanocrystal aspect ratios increase the pitch value in suspensions.[46]

2.4.3. Influence of counterions and ionic strength

The critical concentration for chiral nematic phase formation also depends on the CNC sulphate group counterion type. Monovalent inorganic counterions increase w_0 with increasing atom size, while organic counterions increase w_0 with increasing molecule size. Steric repulsions and hydrophobic interactions between the CNCs explains this.[53]

Dong et al.[36] first observed that the pitch decreases with increasing salt concentration, but only up to a certain concentration, after which the effect is not as clear as it induces aggregation of CNCs. Later Pan et al.[15] and Honorato-Rios et al.[13] confirmed this observation. The charged ions screen the CNC surface charge, lowering the Debye screening length, which enables tighter

packing of the nanocrystals. Electrolyte presence increases the effective aspect ratio by reducing the effective diameter of the nanorods, according to the theory by Onsager,[43] which should increase the pitch. However, salt addition also reduces the effective total volume of the crystals, which results in a reduced pitch value. This effect dominates; thus, the overall effect is a decreasing pitch with increasing salt concentration. Salt addition both increases the onset concentration value of phase separation, but also blurs the phase boundary between the isotropic and anisotropic phase.

2.4.4. Influence of the Solvent

Cellulose nanocrystals are commonly dispersed in water. However, Bruckner et al.[54] showed that self-assembly into chiral nematic phases is also possible in other solvents. Phase separation was observed for CNCs suspended in formamide and N-methylformamide (NMF). Furthermore, the AVF increased with increasing solvent electric permittivity (ε_r), at a specific concentration, while the pitch size measured in the suspension decreased. Therefore, w_0 likely decreased with increasing ε_r. These phenomena can be explanied by an increase in the effective rod volume for decreasing ε_r, as the Debye screening length κ^{-1} decreases.

2.5. Physical effects during evaporation-induced self-assembly of iridescent films

When a suspension of cellulose nanocrystals evaporates, evaporation induced self-assembly (EISA) creates helicoidally structured iridescent films. Whereas the pitch usually is in the range of tens of micrometres in a suspension, when dried, the chiral nematic pitch size of the helix shrinks to a few hundred nanometers.[6] The mechanisms that lead to the formation of solidified chiral nematic structures from equilibrium chiral nematic domains in CNC suspensions during evaporation of the solvent are still poorly understood. This section attempts to clarify the current understanding of EISA.

2.5.1 Kinetic arrest

It has previously been proposed that EISA is a two-stage process.[9,13,55] In the first stage of the evaporation process, chiral nematic tactoids and domains form when the concentration exceeds w_0. The pitch decreases slightly at $w_0 < w < w_1$, and considerably at $w > w_1$.[9,13,51] At a certain concentration, which depends on the surface charge[13] as well as the liquid medium,[9] there is a non-equilibrium stage called kinetic arrest. The suspension starts to gel and the nanocrystal mobility is greatly decreased. The concentration where this happens is defined as w_k.[55] If w_0 is higher than w_k, no liquid crystals form.[29,54] In the second stage of EISA, the high viscosity of the gel hinders the mobility of the nanocrystals. There is a structural collapse when the remaining liquid evaporates, which causes a slight decrease in pitch size.

During EISA, not only the concentration increases, but also the viscosity. Shafiei-Sabet et al.[56] observed that the viscosity behaviour depends on whether w is below w_0, in the biphasic region or beyond w_k, i.e. the viscosity displays a three-region behaviour. This can be used as an approximate measure of kinetic arrest. Honorato-Rios et al.[13] observed that w_k (9-10%) increased slightly as the surface charge increased, for their specific CNCs. Lower surface charges promote network formation and aggregation at lower concentrations.

The work of Mu et al.[9] provides further evidence of this two-stage drying process. By adding D-(+)-glucose into the system, the equilibrium suspension pitch value decreases, which should have produced blue-shifted films with lower pitch values through EISA. However, w_k decreased with increasing glucose amounts. The crystals set in at a higher pitch value when the gelling occured at lower concentrations, and consequently, the films dried from the suspension were red-shifted.

2.5.2. Tactoids and domains

Tactoids are the elementary anisotropic components in liquid crystal suspensions, which can coalesce to form larger liquid crystalline domains when the concentration increases. They spontaneously nucleate in solution into spindles, spherical or ellipsoidal shapes. Tactoids have one or several parallel birefringent bands, corresponding to a 180° turn of the helix and separated by around 10 µm, which can be observed in suspensions by POM as fingerprint lines.[4]

This is an indicator of chiral nematic ordering. Within an elementary tactoid, there is only one orientation of the chiral nematic axis. The size of tactoids vary from a single half-pitch length, to several pitch lengths.[57]

Wang et al.[57] propose the following mechanism for the emergence of solidified chiral nematic ordering during EISA. In drying CNC suspensions, microscopic tactoids start to coalesce and form larger chiral nematic domains. They can fuse by matching chiral nematic axis direction, creating a larger tactoid, which retains the axis direction. Tactoids can fuse even while having different axis directions, creating a multidomain tactoid with several coexisting axes. At the same time, the domains assemble on the bottom of the drying substrate, with the chiral nematic axis perpendicular to the surface plane, creating an ordered lamellar structure.[7,8,14] Defects may form at the contact areas between domains, where the axes are locally tilted. The study was done by capturing the CNC suspension at different drying and concentration stages into a solid polymer matrix, and subsequently investigating with scanning electron microscopy (SEM).[57]

When viewing dried films of nanocrystals in microscopes,[8,17,58] there is usually a mosaic of different colours. Figure 3 shows an example of this polydomain texture, where each coloured region represents a single domain. The reflected circularly polarized light depends on the pitch, the angle of incidence and the refractive index, according to equation 1. As the average refractive index is 1.56 for cellulose,[59] the difference in pitch size or the angle of incidence causes the variation in colour. A chiral nematic domain with a non-orthogonal chiral nematic axis with respect to the substrate reflects light of a lower wavelength compared to a domain with an orthogonal axis, because of the incident angle. Therefore, the variation in colour in Figure 3 could be an effect of varying domain tilts, varying pitch sizes between the domains, or a combination of both.

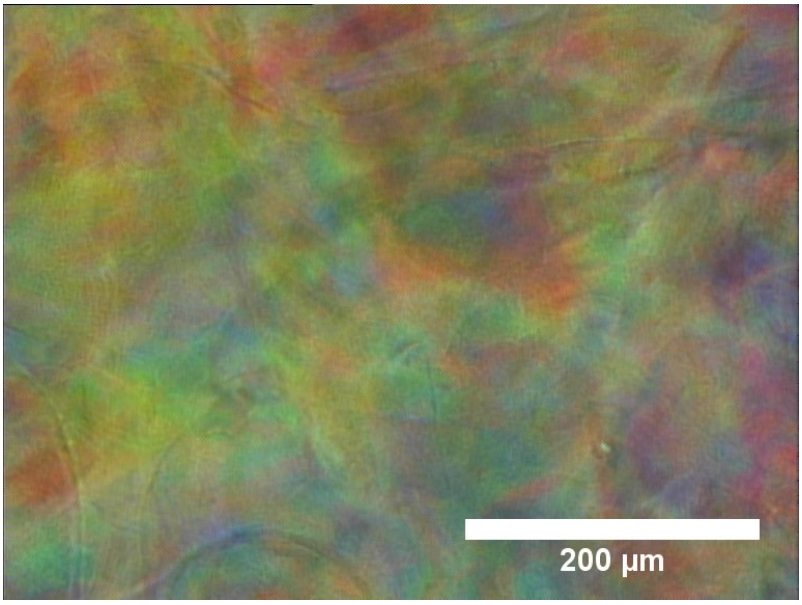

Figure 3. Microscopy image of a CNC film, taken in reflection mode. The mosaic of colours arises from chiral nematic domains, where each domain is responsible for a colour in the image.

Dumanli et al.[8] observed the presence of domains with widths between 2 and 20 µm in a 1 to 2 µm thick dry CNC film. SEM images showed three different pitch sizes corresponding to three distinctly different domains. UV-Vis reflectance spectra of the domains confirmed that the colour mosaic observed in optical microscopy images (similar as in Figure 3) was caused by a difference in inter-domain pitch, not inter-domain axis orientation. Furthermore, Dumanli et al.[8] proposed that the polydispersity in size might cause the formation of domains with different pitch sizes, where the smaller CNCs would produce the smaller pitches and larger CNCs larger pitches. On the other hand, it is possible that each domain would experience kinetic arrest[9] at a different stage, in which case the domains that gel earlier would have larger pitch sizes.

Park et al.[14] studied the effect of the initial AVF and shearing on the orientation of the chiral nematic domain axes. According to their theory, when either the whole or part of the suspension is isotropic, then the domain axes will adopt a random orientation. The random orientation is preserved until kinetic arrest, after which the chiral nematic axis does not change anymore. Starting the EISA above w_1 would prevent the formation of a multi-coloured structure in the dry film, which is caused by the domains each having a different axis orientation. Park et al.[14] assumed that for $w > w_1$, the whole liquid would consist of a single large domain with the axis orientation orthogonal to the substrate. This orientation would be preserved during gelling and

therefore also in the dried solid film. POM images showed that the colour was more uniform when dried from above w_1 than when dried from below w_0, and the areas displaying a specific colour were larger. SEM images confirmed a uniform pitch size and an orthogonal helix axis.

2.5.3. Drying rate and mechanism

Previous sections described the fundamentals of CNC liquid crystals and chiral nematic structures forming through EISA, regardless of the evaporation rate of the liquid phase. This section covers the effect of the temperature and drying rate on colour and pitch size in dried films, as well as the movement of CNCs in a drying suspension.

Beck-Candadedo et al.[5] observed a red-shift in CNC films dried at higher temperatures, compared to films dried at lower temperatures. Tang et al.[60] observed a red-shift in films dried at lower pressures (sub-atmospheric), compared to films dried at higher pressures. In both cases, the evaporation rate increased for the EISA resulting in the red-shifted films. When the evaporation rate is faster, there is less time for the chiral nematic pseudo-planes to diffuse towards each other as water is lost, and they are locked in a wider structure as the structure reaches complete dryness. This leads to elevated pitch and lower density. In contrast, Pan et al.[15] observed the inverse effect on pitch with increasing drying temperature (blue-shifted films), but there was no clear explanation for this behaviour. Similarly, Dumanli et al.[6] discovered this inverse effect, by altering the evaporation rate through varying the environment humidity. Liu et al.[48] found that films dried at a temperature above 70°C did not display any chiral nematic order. The reason could be desulfation, which is initiated above 40-45°C.[29]

Beck et al.[5] observed peak broadening in films dried at elevated temperatures, compared to films dried at lower temperatures. In this case, the chiral nematic domains that form during the drying might be more disordered, either in pitch size, or in chiral nematic axis orientation. Both would cause a broader reflection peak. The CNCs in the liquid crystalline phase are on average perpendicular to the chiral nematic orientation axis, but some of the crystals are always slightly out-of-plane due to thermal motion. This effect might be pronounced with higher drying temperature, which effectively could lead to a larger film pitch variation.[5,14]

CNC films can be patterned with varying colour by selectively applying a heat gradient to the desired film pattern area during evaporation. As expected, the area exposed to higher temperatures during the evaporation display red-shifted reflection with respect to the unexposed areas. The patterning also works in the opposite way, by cooling an area of the film during drying, a blue-shift and lower thickness can be observed in the patterned area.[5]

During the evaporation of water from a cast CNC suspension, the concentration will steadily increase, and the CNC particles will accumulate at the liquid-air interface. This results in a decrease in surface tension at the interface and the formation of a skin,[42] which decreases the evaporation rate and local time-dependent concentration in the middle part of the liquid volume.[17] Generally, the top part of a CNC film is more disordered, while the bottom part displays more defined helical order, where the chiral nematic axis is orthogonal with the substrate plane.[7,22,24,57] As the top skin part reaches kinetic arrest faster,[9,55] the structure in locked into a disordered state, while the bottom part has more time for self-assembly into ordered chiral nematic structures.

Jativa et al.[42] studied the movement of CNCs inside a shrinking water droplet, effectively simulating the drying of a CNC suspension during EISA. The CNCs behaved differently depending on the droplet shrinkage rate (drying rate). Although the nanocrystals used in this study did not contain sulphate surface groups and therefore did not form chiral nematic liquid crystals until after several months, this study may still provide valuable insights into the drying mechanics during EISA. At a low shrinkage rate, tactoids formed in a controlled manner, and subsequently coalesced into birefringent microbeads. On the other hand, at a high shrinkage rate, the radial diffusion of CNCs away from the droplet surface could not compete with the droplet shrinkage, which led to high CNC concentration gradients at the suspension interface. In this case, tactoids near the interface formed a stable birefringent shell. In addition, the high shrinkage rate resulted in larger microbeads than if formed at the lower shrinkage rate. However, the formed microbeads showed neither a cholesteric arrangement nor iridescence. Nevertheless, the results of the study may suggest that the skin formation and the degree of disorder in the top part of a dried film could be enhanced by using faster drying rates.

2.5.4. Coffee-ring effect

Whereas previous sections focus on the formation of helical order on a smaller scale, this section covers the formation of colour on a macroscopic scale. Here the whole drying suspension volume will be covered. There are yet challenges to obtain dry CNC films with an even colour throughout the film area, due to the coffee ring effect.

In sessile droplets shaped from CNC suspensions drying on a flat surface, the evaporation of water is faster at the edges of the droplet than at the centre. If the contact line is pinned during the evaporation, this leads to a radial particle capillary flow towards the perimeter.[61] The radial particulate flow causes a thickness variation in the film, and a valley forms in the centre of the film. The central part is thinner and gets thicker when moving radially towards the edges of the dried film. Furthermore, gelling[9,55] occurs at a lower CNC concentration and higher pitch at the edges, where the evaporation rate is higher. Consequently, the centre of the dry film becomes bluer, while the film becomes increasingly red-shifted towards the edges. Figure 4 shows this radial change in reflected wavelengths. Mu et al.[62] observed a decrease in the radial thickness variation when increasing amounts of glucose were added to the suspension prior to EISA. The viscosity increase may inhibit the particulate movement towards the edges, and therefore counter the coffee-ring effect.[17,62]

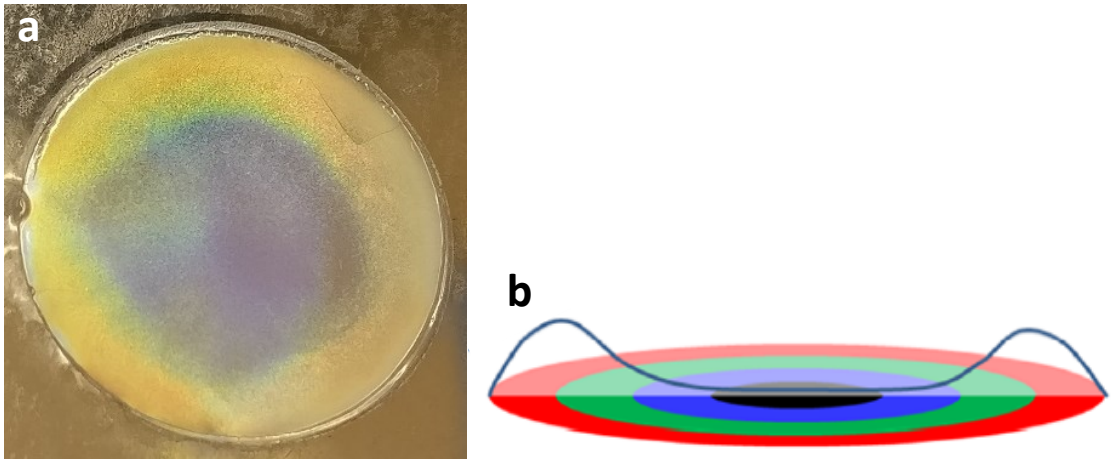

Figure 4. (a) The radial colour difference in the displayed CNC film is caused by the coffee-ring effect. (b) Schematic of the coffee-ring effect, where the differential drying (faster towards the edges) causes particles to migrate towards the edges, and the film becomes thicker towards the edges. The differential evaporation rate also causes the colour difference.[62]

The Marangoni effect counteracts the coffee-ring effect by causing a particulate flow towards the centre. The surface tension is higher at the centre of the meniscus than at the edges, which results in shear stresses responsible for the particulate flow. Gençer et al.[17] calculated the Marangoni numbers for CNC suspension volumes, by using the derivative of the surface tension (suspension/air) with respect to the change in concentration, and using constants (viscosity, droplet diameter and particle diffusivity). At low (0,6%) initial CNC suspension concentrations, the Marangoni flow number was higher than in higher CNC suspension concentration (3,7%). This led to higher solid fractions being deposited at the edge than at the centre, in films dried from higher initial CNC suspension concentrations. Therefore, sessile droplets of CNC dried from 0,6% suspensions exhibited a very uniform thickness. However, they did not display iridescence due to the low film thickness. Furthermore, subjecting the evaporating suspension to an ethanol environment amplified the Marangoni effect, due to the surface tension loss when ethanol flowed into the suspension volume. This gave an even radial solid deposition in the dried film, but the ethanol in the system disrupted the chiral nematic ordering, increased aggregation and inhibited structural colour formation.[17]

2.5.5. Shear relaxation

Gray et al.[63] observed a highly concentrated CNC suspension in POM, after applying a shearing force (by pressing the suspension between two glass slides). The initially chiral nematic liquid crystalline phase adopted a more nematic-like orientation post-shearing. During the next 18 hours, the suspension relaxed and re-adopted the chiral nematic texture, while the concentration was constant. Two different relaxation mechanisms were proposed, as depicted in Figure 5. In the mechanism shown on the right, only the chiral nematic pseudo-planes moved relative to each other to align from an infinite pitch (e) into the equilibrium pitch (c). In the newly proposed relaxation mechanism shown on the left (a to c), the nanocrystals tilt relative to the nematic director, in addition to the relative chiral nematic pseudo-plane movement.

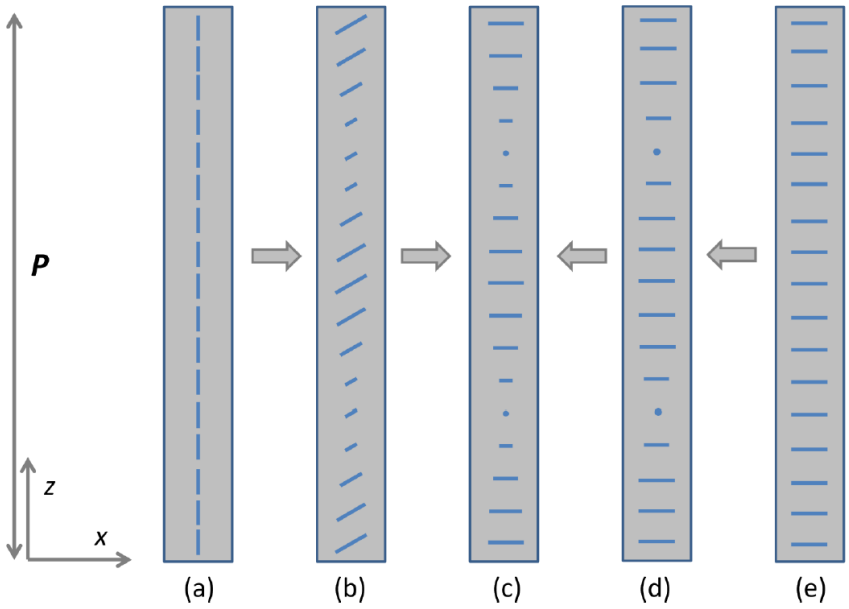

Figure 5. Two different shear relaxation mechanisms. Image in (c) represents CNCs (lines) in a relaxed state in suspension, where they adopt a chiral nematic orientation. z represents the direction of the chiral nematic axis and x the direction of the director of the CNCs at 180° intervals. Both (a) and (e) represent CNCs in suspension in a nematic orientation after the suspension has experienced shear. The CNCs undergo shear relaxation back into the chiral nematic orientation either through a →b →c or through e →d →c. a →b →c is a twist-bend relaxation mechanism proposed by Grey et al.[63]

2.5.6. Vacuum-assisted self-assembly

Iridescent CNC films with chiral nematic ordering have been produced though a vacuum-assisted filtration, where a Buchner funnel system was utilized to drain the water through a filter paper. In contrast to the film casting technique (EISA), the initial suspension was relatively dilute (1%) and a 10h bath sonication prior to the film formation was required to obtain iridescent films through vacuum-assisted self-assembly (VASA).[60]

2.6. Controlling pitch and chiral nematic order in films formed through evaporation-induced self-assembly

This section discusses the control of the pitch and the uniformity of the helical order in CNC films by altering the conditions of the evaporation-induced self-assembly by other means than

controlling the evaporation rate. In addition, this section covers the effect of altering the state of the suspension prior to EISA.

2.6.1. Controlling the pitch through the initial suspension state

Sonication of CNC suspensions may affect the CNCs in a multitude of ways. Previous studies have reported the effect of high energy input tip sonication. Dong et al.[29] observed that the average length of the CNCs decreased with increasing sonication input, whereas the surface charge remained more or less constant. They further reported an increase in w_0, which has also been reported by Beck et al.[49] Theory of Onsager[43] would explain the increase in w_0, assuming that the CNCs broke by splitting, the width of the CNCs remained constant and thus the aspect ratio decreased. Liu et al.[48] observed a decrease in the length, width and surface charge of CNCs treated with increasing sonication input. In contrast to the previous report by Dong et al.,[29] the CNCs might have been reduced in size also due to peeling off of surface layers. This would explain the reduction in surface charge, as new surface without charged sulphate groups would be uncovered.

Beck et al.[49] reported an increase in the pitch size of CNCs in suspension, as an effect of increasing sonication input. The increase in pitch size have resulted in red-shifted films when the suspensions have been dried.[48,49] In the study by Liu et al.,[48] the aspect ratio did not change much but the surface charge decreased, which would explain the increase in pitch size.[51] Beck et al.[49] proposed another explanation to this pitch size reduction, when detecting an increase in the conductivity of a CNC suspension after sonication. The sonication would release ions trapped in the bound-water layer in the CNCs, which would expand the electrostatic double layer surrounding the CNCs and increase the pitch. In addition to a red-shift, Liu et al.[48] also detected a wider reflection band-width for the CNC films dried from more extensively sonicated suspensions. In addition to being smaller, the size distribution was more polydisperse. Films produced from more polydisperse suspensions might contain a wider distribution of domains, having different pitch sizes and orientations. The polydomain organization would lead to a wider reflection spectrum.

Adding salt (herein NaCl) reduces the pitch size in suspension, in addition to increasing w_0 (see section 2.4.3.). This reduction in pitch can be preserved through EISA, to obtain blue-shifted

films. Pan et al.[15] observed a blue-shift of the average pitch with circular dichromism (CD) in films dried from suspensions with added salt. However, there was a larger scatter of the pitch values and the CD spectra were wider.

Liu et al.[48] observed that the thickness of iridescent CNC films did not affect the peak reflection wavelength. However, it did affect the peak reflectance intensity. Thicker films produced higher reflection intensities and narrower bandwidths in the range 42-96 µm. This can be understood using a multilayer interference theory explanation.[34] The CNC films are a multiple of thin films stacked on top of each other. Increasing the number of layers decreases the bandwidth, as the refractive index differences between the layers is very small. Beck et al.[5] did not detect a difference in pitch when varying the film thickness.

2.6.2. Controlling the alignment of CNCs using shear forces

Without external forces, cellulose nanocrystals assemble into chiral nematic order when cast from suspensions. Whereas the chiral nematic arrangement is more difficult to externally control, it is possible to align the CNCs in a nematic arrangement, by e.g. electric or magnetic fields, or by shear forces. Hoeger et al.[64] investigated variables influencing the alignment of nanocrystals films cast using a withdrawal plate. At concentrations above 2,5%, on gold or silica substrates carrying adsorbed polyethylene imine (PEI), films were produced where 40-60% of the crystals were aligned within 20° from the direction of shear.

While a linear shear flow disrupts the chiral nematic self-assembly in favour of a nematic arrangement, a circular shear flow can aid the chiral nematic axes to align more uniformly in an orthogonal orientation with respect to the substrate, during EISA. Park et al.[14] concluded that a left-handed circular shear applied during EISA is especially effective when the CNC suspension is fully isotropic. This was done using an orbital mixer moving in a circular manner (not rotating) at a speed of 40 rpm. The chiral nematic axes of the tactoids that form when the concentration rises above w_0 are oriented in random directions.[4] When a horizontal shear flow was applied, a vertical orientation for the chiral nematic axis became more prevalent. SEM cross-section images and POM images revealed that most of the helical axes were indeed vertically aligned, although there was pitch size variations. When the same experiment was done with a suspension with an initial concentration between w_0 and w_1, the domains in the dried films were

aligned less uniformly in the vertical direction. The shear flow in EISA may not align tactoids that already exist in the suspension prior to EISA as easily as it aligns newly forming ones.

The evaporation-induced particulate motion inside a drying suspension creates a vertical concentration gradient which increases towards the surface. The surface layers of dried films have been observed to be more disordered and having larger pitch values. Weak circular shear flow (orbital mixer, 44 rpm, see above paragraph) applied during EISA can address this problem. The concentration gradients are cancelled out by the shearing and the kinetic arrest delayed in the surface layer, resulting in a more homogeneous film throughout the thickness.[7]

2.7. Reversible colour change in dried films

Dry chiral nematic films can reversibly adopt a new colour when subjected to water or high humidity. The water penetrates the chiral nematic domains, and elevate the pitch due to the swelling of pseudo-planes. Zhang et al.[20] observed a colour change from blue-green to orange-red in a dried CNC film when adding water. The speed of the colour change depended on the thickness of the film. This phenomenon could be utilized to produce a humidity sensor.

2.8. Composites and templating

Mixing CNCs with another component prior to EISA has been studied thoroughly. The additional components can be agents for plasticising,[24-26,65] modifying the colour[24-26,65,66] or improving the stability[24,66] effects on the subsequently dried films. PEG increases the flexibility and ductility of CNC films, but weakens the composite.[24,25] It red-shifts the film[24,25] by penetrating between the chiral nematic pseudo-layers. In excess, PEG can disrupt the self-assembly, resulting in heterogeneous colouration. PVA[65] and (dimethylmyristylammonio)propanesulfonate (DMAPS),[26] a zwitterionic surfactant, have the same effect, improving the toughness and ductility, and red-shifting the films. In contrast, polyacrylate (PAAS) additions blue-shifted the films.[24] Silica precursors can be cross-linked inside CNC suspensions, to obtain silica/CNC composites after EISA. These have higher pitches than pristine CNC films, and improved heat and moisture stability.[66] Furthermore, the CNC can be removed from the dry film by alkaline treatment[66] or burning.[18] The chiral nematic helical order is preserved in the CNC-templated silica film, where the pitch is reduced when the CNC is

removed. The pitch size of the templated silica film can be delicately tuned by altering the CNC/silica ratio.[18]

3. EXPERIMENTAL

This part of the thesis lists the materials and chemicals used and then describes all the methods and procedures used to complete the experimental laboratory work. It includes initial work that was made for troubleshooting purposes, aiding the subsequent studies. This work is found in the initial section under the methods section. There are two studies with meaningful results, related to the effect of temperature and the concentration. Finally, the experimental section includes characterization methods that were used in the initial work and the two studies.

3.1. Materials

Nanocrystals used in the preliminary conditions optimization work (section 4.1.) were made from Whatman 1 cotton filter paper. The nanocrystals used in later work (section 4.2 and 4.3) and partly in the preliminary conditions optimization work (section 4.1.) were purchased from the Process Development Centre in the University of Maine, U.S.A, as a 11,1% (w/w) aqueous suspension. They were produced at the USDA's Forest Products Laboratory (FPL, Madison, WI). The sulphur content given by the producer was 0,095 wt%, corresponding to 297 mm/kg. Millipore (Synergy UV) milli-Q water was used for dilution. Ethanol (A, 94%) was obtained from Altia Oyj.

3.2. Cellulose nanocrystals production and concentration for the preliminary conditions optimization

Marja Kärkkäinen thankfully performed the CNC production work described in this section. The cotton filter paper fibres were ground with a Wiley Mill. 15 g of ground fibre powder was placed in a round-bottomed flask into a 50°C water bath. 64% sulphuric acid was added and the reaction mixture was stirred for 2 hours, after which the reaction mixture was added to 3 l of water to end the hydrolysis reaction. The CNC dispersion was left to settle overnight after which excess acid was poured out. The remaining CNC containing fraction was centrifuged once with a Wifug original centrifuge and once with a Mitsubishi U100 centrifuge. The CNC was dialyzed for 64 h until the conductivity of the dialysis water was less than 5 µS/ml. The purified CNC

dispersion was filtered using a Whatman filter paper, to remove any overly large particle fractions. Approximately 1.5 ± 0.5 % (w/w) CNC suspensions were obtained using this method

The dry-weight of the CNC suspension was measured and the suspension was placed in a sealable glass bottle. It was placed in a Thermo scientific vacuum oven without the lid but covered with a nylon fabric to prevent dust and dirt from entering the bottle. Water was slowly evaporated from the bottle at 50 mbar and 42°C until the concentration reached 3% (w/w).

3.3. Procedure for the film formation through altering the evaporation temperature

Cellulose nanocrystal suspensions were solvent cast at varying evaporation temperatures to obtain dried films of nanocrystals. The experiments performed in this section utilizes the 11.1 % (w/w) CNC suspension obtained from the University of Maine, U.S.A. The films characterizations are presented in sections 3.5.1. (visual observations from photographs) and 3.5.2. (UV-Vis spectroscopy).

A special set-up was used for the solvent casting, seen in Figure 6, where a Precisa 205ASCS scale was placed inside a closed Memmert oven. The samples were solvent cast at constant temperature inside the oven, while the weight of the CNC suspensions was measured at 30 second intervals, to correlate the loss of water with time. The evaporation rate was then correlated with the optical properties of the dried films.

Figure 6. The setup used to measure the weight change (loss of water) in drying CNC suspensions, against time. The samples were placed, one at a time, inside the scale, which collected data during the course of evaporation. The oven door was closed during the experiment.

The 11,1% CNC suspension was diluted to 3% simply by adding milli-Q water and mixing thoroughly. 4 ml of the suspension was pipetted into Greiner bio-one polystyrene (diameter: 3,5 cm) Petri dishes. The temperatures used for the solvent casting were 23, 28, 36, 41, 51 and 61 °C, and the corresponding samples were denoted T23, T28, T36, T41, T51 and T61. The weight loss was not measured from the T51 and T61 samples. The Petri dishes containing CNC suspension were placed on the scale inside the oven and the weight measurement against time was started in the pre-heated oven. The sample names and casting conditions are listed in Table 1, which also contains samples used in section 3.4.

Table 1. Sample names and casting parameters for the procedures in sections 3.3. and 3.4. The amount of nanocrystals is constant in each film, approximately 120 mg.

Sample	Equilibration days	Casting suspension concentration and volume	Substrate treatment	Casting Temperature
T23	0	3% 4 ml	no treatment	23°C
T28				28°C
T36				36°C
T41				41°C
T51				51°C
T61				61°C
NE_w3	0	3% 4 ml	Ozone/Water	21°C
E_w3	7			
NE_w4	0	4% 3 ml		
E_w4	7			
NE_w5	0	5% 2.4 ml		
E_w5	7			
NE_w6	0	6% 2 ml		
E_w6	7			
NE_w7	0	7% 1.71 ml		
E_w7	7			
NE_E3	0	3% 4 ml	Ozone/Ethanol	
E_E3	3			
NE_E4	0	4% 3 ml		
E_E4	3			
NE_E5	0	5% 2.4 ml		
E_E5	3			
NE_E6	0	6% 2 ml		
E_E6	3			

3.4. Procedure for the film formation through altering the initial concentration

This work focusses on the effect of the initial solvent casting CNC suspension concentration on the colour properties of the dried films. CNC suspensions of five different concentrations were solvent cast in treated Petri dishes in two different conditions for each concentration. The experiments performed in this section utilizes the 11.1 % (w/w) CNC suspension obtained from the University of Maine, U.S.A. The characterization methods for this work is presented in section 3.5.1. (visual observations from photographs), 3.5.2. (UV-Vis spectroscopy), 3.5.3. (optical microscopy and SEM).

The Petri dish substrates were surface treated to improve the interaction between the CNC suspension and the substrate. They were placed in a Bioforce Nanosciences UV-Ozone oven for 30 min and subsequently washed with either ethanol or water (ion-exchanged), to obtain two slightly different surfaces. The static contact angles on the pristine and the two treated substrates was measured using a KSV CAM 200 optical contact angle meter. A 7 µl water droplet was used.

The initial 11.1% (w/w) CNC suspension was diluted with milli-Q water to 1, 2, 3, 4, 5, 6 and 7 % (w/w) suspensions. Equal volumes of each concentration were placed in long cylindrical glass vials (diameter 2.6 cm, height 12.5 cm). After one, five and 14 weeks, the contents of the vials were visually observed, to determine the position of the phase boundary. The distance from the bottom of the liquid volume to the phase boundary was measured, and related to the total height of the liquid volume. As a result, the anisotropic volume fraction was obtained for each concentration of the suspensions.

Suspensions were cast in Petri dishes (diameter = 3.5 cm) and films were obtained by drying in room temperature (21°C and 20% humidity). Three different parameters were varied: the concentration (3, 4, 5, 6 and 7%), the substrate (untreated, ozone/ethanol treated and ozone/water treated), and the equilibration time (no equilibration, 3 days and 7 days). The sample names and casting parameters are listed in Table 1. The casting volume was adjusted for each specific concentration condition so that each film would contain 120 mg of nanocrystals. therefore, the drying time differed with each concentration condition. However, the drying time was not accurately measured. Equilibration was achieved by covering the suspension-containing Petri dish substrate with a lid to isolate the suspension and preventing it from drying, prior to the actual drying.

3.5. Characterization

3.5.1. Properties of purchased cellulose nanocrystals

CNCs purchased from the Process Development Centre in the University of Maine were characterized by pH measurement, dynamic light scattering and zeta potential measurement. A Mettler Toledo SevenEasy pH meter was used to measure the pH at 25°C in a 5,5% suspension.

A Malvern nano Series Zetasizer was used to obtain the zeta potential, by diluting a CNC suspension to 0,25%, containing 10 mM sodium chloride. A Malvern Nano Series Zetasizer device was used to obtain an apparent CNC size by dynamic light scattering, using a 0,025% CNC suspension. Table 2 lists the characterized properties. The pH value is higher than what is usually reported for CNCs produced in the laboratory. The suspension may have been neutralized with sodium hydroxide after the hydrolysis, as reported by Fu et al.[67] (Polymers, 2017, 9). This suggests the CNCs would be in the sodium form. The zeta potential value (-32,7 mV) was smaller than values previously obtained for the same CNCs, but still large enough for colloidal stability.[27,67-69] The sizes according to the DLS results were similar as those measured before by Reid et al.[27] (55-60 nm).

Table 2. Properties of CNCs purchased from the Process Development Centre in the University of Maine.

pH (25°C)	Zeta potential, mV	Average particle size by DLS, nm
6,6	-32,7	68,5

3.5.2. Photographs

Photographs of the T23, T28, T36, T41, T51, T61, NE_w3, E_w3, NE_w4, E_w4, NE_w5, E_w5, NE_w6, E_w6, NE_w7, E_w7 samples were taken with an OnePlus 3 mobile phone camera, by placing the films on a black background. The photographs were taken from the base of the films, through the transparent Petri dish substrate.

Photographs of the NE_e3, E_e3, NE_e4, E_e4, NE_e5, E_e5, NE_e6, E_e6, NE_e7, E_e7 samples were taken with a Nikon D7200 camera against a black background. The photographs were taken from the base of the films, through the transparent Petri dish substrate.

3.5.3. UV-Vis spectroscopy characterization

The samples solvent cast on glass slides and in Petri dishes were characterized by a Perkin Elmer lambda 950 Uv/Vis spectrometer. Transmittance spectra were obtained in the wavelength range 300 to 800 nm.

Printing paper was printed black on one side and 5,5 mm diameter holes were made in 2,6 cm times 5 cm pieces of the papers. In the case of the samples prepared on glass slides (see section 4.1), the pieces were fastened onto the sample side of the glass slides such that the holes were above the centre of the films, and the white side of the paper was in contact with the glass. The glass slides were then placed in the sample holder so that the black paper side was facing the incoming light. The paper limited the incoming light to area the circle, while absorbing the rest. The reference background was measured with a glass-slide without sample, but with the black paper cover. Each sample was then measured once.

In the case of the Petri dishes from the temperature and concentration studies, a slightly different set-up was used. The reference glass-slide used for background measurement in the previous set-up was placed in the sample holder, on the side facing the incoming light. The Petri dish containing the dried film was then placed on the opposite side of the sample holder, with its bottom facing the incoming light. Therefore, the light exiting the device first hit the masked black paper, then the Petri dish bottom, and finally the film deposited on the Petri dish. The reference background was measured with an empty Petri dish. Three points were measured for each Petri dish sample, by rotating the dish in place. The points were measured from the middle region of the film, at an equal distance from the centre point of the Petri dish. Using Origin software, the average spectrum was obtained from the three spectra for each film.

3.5.4. Optical and scanning electron microscopy characterization

Optical microscope images were taken at 10 times magnification using a Leica DM4500 P microscope in reflection mode.

The film-containing Petri dishes were fractured in half to observe the cross-section fracture surface of the CNC films. The E_w3, NE_w6 and NE_w6 sample films were sputtered to create a 4 nm thick platinum coating on the fractured surfaces. The samples were imaged in a Sigma Zeiss ULTRA-plus Scanning Electron Microscope (SEM). The pitch was measured from the E_w3, NE_w6 and E_w6 films characterized in SEM. Six measurement points in a zoomed-in bottom part of each film was used to obtain an average pitch size and a corresponding scatter value. However, they are approximate, because it is challenging to find two points where the nanocrystal directors

are strictly equal, and also because the chiral nematic pseudo-planes could be non-parallel with the axis of observation.[70] Previous work has suggested that measurement problems related to tilted axes can be addressed by measuring the lowest pitches only. This procedure was used only for E_w3, because the pitch differences in NE_w6 and E_w6 could stem from real pitch differences related to stratification or domain formation.[8] Therefore, the pitches from the whole image were measured for the NE_w6 and E_w6 films, whereas only the upper section, with lower brightness, was used for E_w3.

4. RESULTS AND DISCUSSION

4.1. Preliminary conditions optimization

This section presents preliminary work conducted to investigate the film-forming behaviour of liquid crystalline CNC suspensions. CNC suspensions were solvent cast on glass-slides and in Petri dishes at various amounts to visually observe how the structural colour, arising from the helical chiral nematic order, formed in the iridescent films.

Here, in contrast to later work, laboratory produced CNCs were used. There were several reasons for concentrating the dilute, approximately 1.5 ± 0.5 %, CNC suspension prepared from the Whatman 1 cotton filter paper. In initial EISA attempts, glass-slides substrates were covered with laminate to restrain the suspension to a 1,5 cm diameter circular area cut out from the laminate. As this limited the liquid volume, a 3% suspension was needed to get a thick enough film. Furthermore, using 3% instead of 1,5% suspensions in the solvent casting reduced the EISA time by half.

Figure 7a displays a film made from the concentrated CNC suspension (prepared from filer paper in the laboratory), by drying 300 µl in room temperature for 4-6 hours. The iridescent colour of the film arises from the selective reflection of left-handed circularly polarized light in the visible wavelength range.[35] The contact line remained pinned during the evaporation, i.e. the area of the suspension in contact with the glass slide remained constant. There is a clear radial colour change from the centre to the edge in the dried film (Figure 7a). This phenomenon is usually observed in EISA of droplet-shape CNC suspensions where the contact line is pinned. The coffee-ring effect[61,62] causes this due to a differential drying at the edge and the centre of the film. Therefore, the centre of the circular film is blue-shifted, while the edge is red-shifted, as shown by the illustration in Figure 7b.

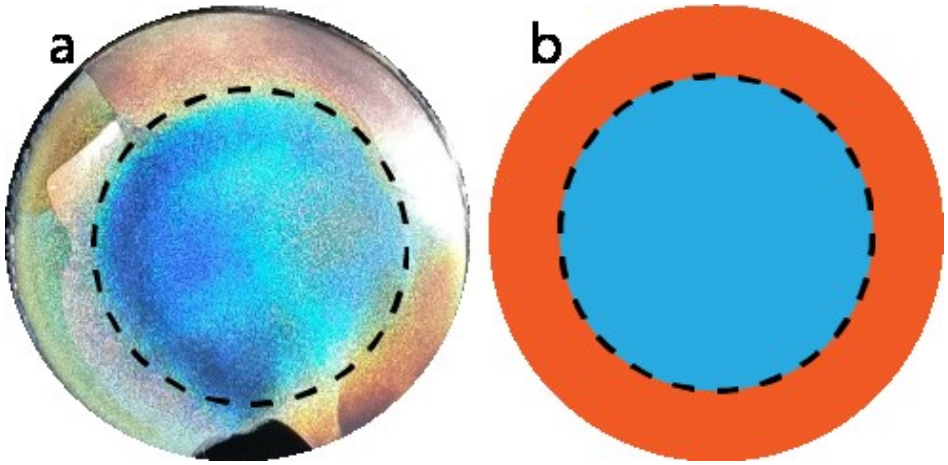

Figure 7. (a) A CNC film dried on a glass-slide from a 3% suspension, and (b) an illustration of the radial colour distribution appearing due to the coffee ring effect.[62]

When these films assembled on glass slides were characterized by UV-Vis, the resultant spectra did not differ very much between the samples (Figure 8). According to the results of Beck et al.,[5] the films should red-shift when dried at higher temperatures. Nevertheless, there are some small differences in the shape of the spectra. At closer observation, there is a change in the slope of the spectra at around 500 nm for the green spectrum, and 575 nm for the red spectrum, indicating some small drying temperature dependence of the reflection colour.

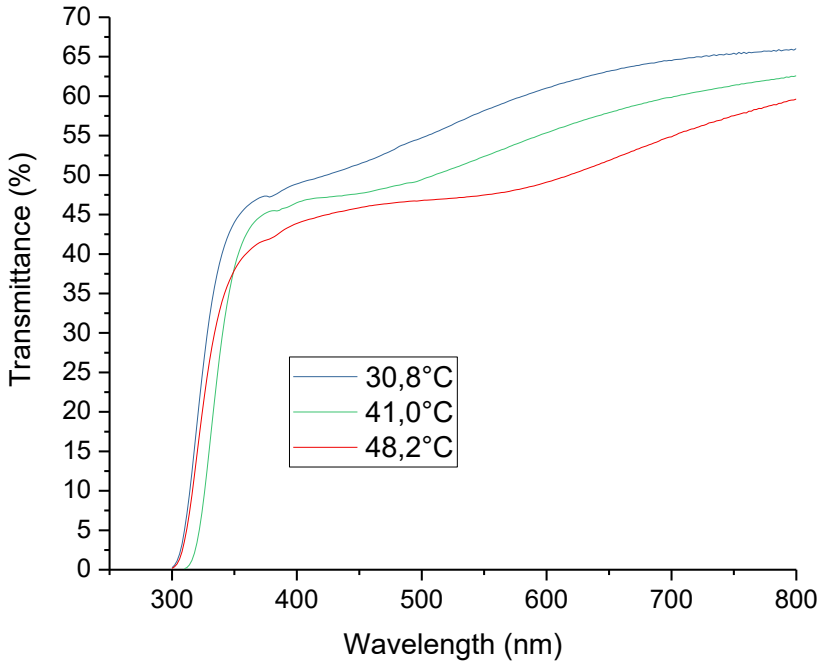

Figure 8. UV-Vis transmission spectra of films dried on glass slides, at different temperatures. Altering the drying temperature is expected to affect the colour according to Beck at al.,[5] However, from the spectra results, the colour was very similar in these films.

The laminate 1,5 cm cut-out limited the film area. The volume constraint resulted in a thickness constraint in the dried film, which in turn prevented obtaining good transmission spectra in UV-Vis characterization. Using Petri dishes as the substrate instead of glass slides solved the above-mentioned issues. Enough liquid could be pipetted into the Petri dishes to obtain dry films that were thick enough to get good UV-Vis data, shown in Figure 9. Furthermore, the substrates did not need to be laminated prior to EISA, thereby saving time. Therefore, Petri dish substrates were used in the subsequent work.

Whereas the spectra for the films dried on the glass slides did not provide any information about a reflectance wavelength or wavelength bandwidth, the Petri dish sample clearly showed a quantifiable maximum in reflectance (minimum transmission) at around 550 nm (Figure 9). Prior to EISA of the two samples, the ratio of liquid per unit area was approximately 3 times higher for the Petri dish sample. This should give a thicker sample, which could provide an explanation for the difference in the spectra. Liu et al.[48] found that too thin, 42 µm, CNC films didn't provide any distinguishable peak in reflectance measurement. However, when increasing the thickness up to 96 µm, increasingly distinguishable and quantifiable peaks appeared. This is in accord with the spectra of Figure 9.

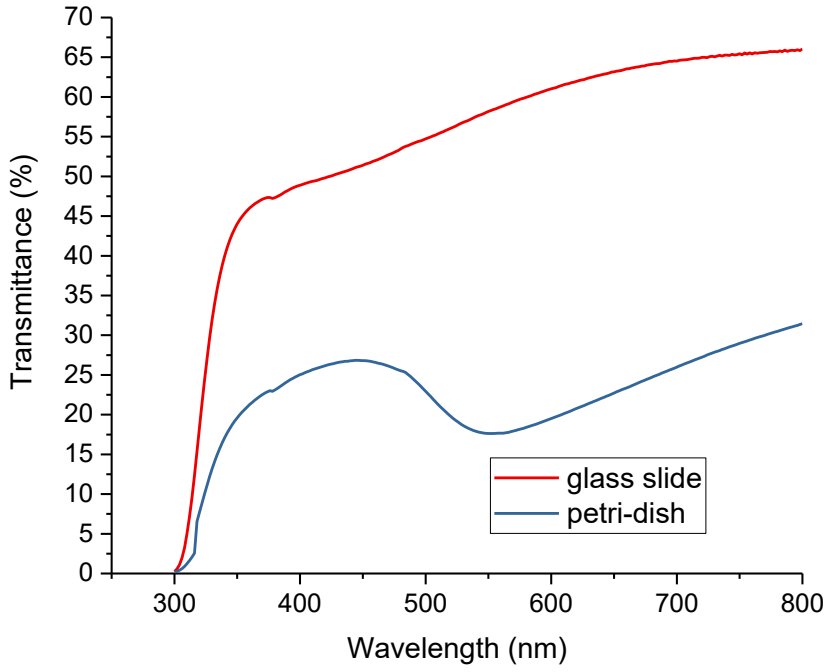

Figure 9. UV-Vis transmittance spectra measured from a film dried on a glass slide and from film dried on a Petri dish. The film dried on the Petri dish was detached and attached on a glass-slide before the measurement, to get comparable spectra. Both films were cast from the same starting CNC suspension and dried at the same conditions. In order to obtain useful data from the UV-Vis spectra, there needs to be a "valley" in the spectrum, which should correspond to the maximum reflectance of the film. In this case, only the film dried on the Petri dish gives a useful spectrum.

Around the time when Petri dishes were chosen as the main substrate, a large quantity of a new cellulose nanocrystal suspension was externally obtained. This highly concentrated 11,1% (w/w) suspension produced, after dilution, iridescent films through EISA (Figure 10). This new starting material was used in later work, simply because it was much more abundant, and also because dilution was much easier than concentration, in order to obtain specific concentrations, up to 7%.

Figure 10 shows the considerable difference in films formed on glass-slides (Figure 10a) and on Petri dishes (Figure 10 b, c). In contrast to the film in Figure 10a, the film in Figure 10b and 10c formed from 4 ml of the externally obtained CNCs, diluted to 3%. Therefore, Figure 10a and Figure 10b are not fully comparable. It is worth noting that the area of the Petri dish sample (Figure 10 b, c) is more than 5 times larger than that of the glass slide films (Figure 10a). The drying mechanics of a sample dried in a cylindrical container is different from one dried on a flat surface. The glass slide film (Figure 10a) dried from a droplet-shaped volume, causing nanocrystals to diffuse towards the edges.[17,62] Consequently, the red-shifted edge was expected to be thicker, while the central blue area was expected to be thinner. Suspensions drying in Petri dishes also covered the edges of the dish, creating a layer of dry CNC on the edges. Capillary forces and residual stress[71,72] caused a crack to form near the outer ring of film. Furthermore, there was no clear radial colour evolution.

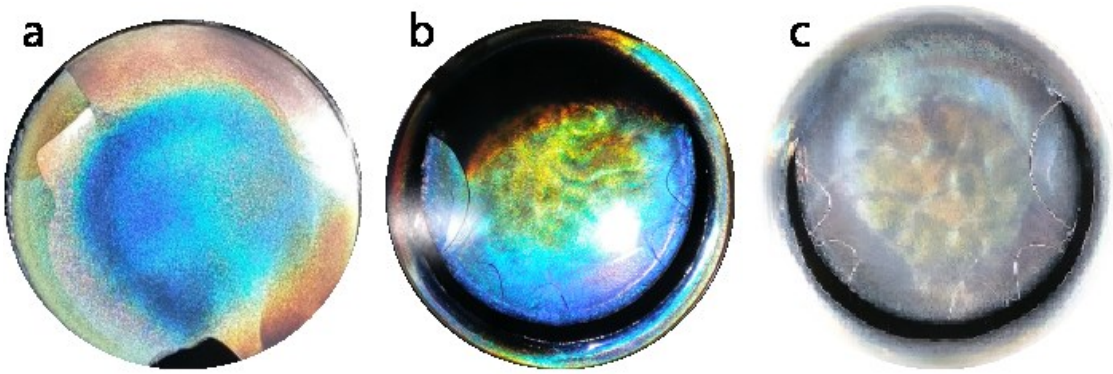

Figure 10. (a) Photograph of a film dried on a glass slide, identical to Figure 7a. (b, c) photographs of a film dried in a Petri dish (diameter = 3.5 cm). Photographs (a) and (b) were taken using a camera flash, in a dark environment, while photograph (c) was taken with light sources at the sides.

The effect of initial concentrations was also investigated. Samples were dried from a three and six percent suspension, but the volume was varied in order to keep the total solids constant (120 mg). Figure 11 reveals that the concentration influences the visual appearance of the film (Figure 11 a, b), and the spectra obtained in UV-Vis (Figure 11c). The spectra reveal a blue-shift for more concentrated suspensions, as well as a spectral broadening. The circular crack that appeared in all samples dried in Petri dishes appears to be much larger in the 6% sample. There is an asymmetrical deposition of nanocrystals towards one edge. The direction was found to be random. The difference in crack size could stem from a difference in the build-up of residual stress[71,72] during EISA. The effect of concentration was considerable and therefore this effect was studied in depth, in section 4.3.

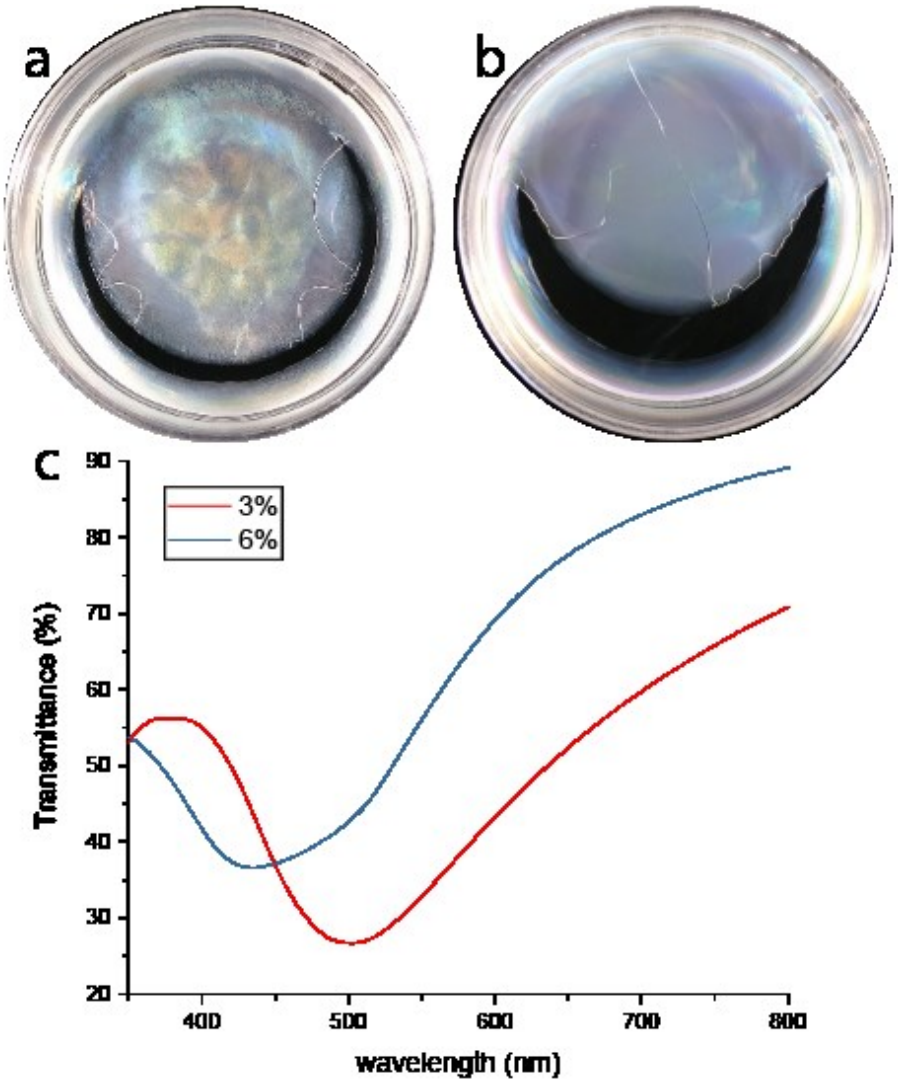

Figure 11. Films dried in Petri dishes, from (a) 3% (4 ml), and (b) 6% (2 ml) CNC suspensions. The 3% film is more centered in the Petri dish. Transmission spectra (c) for both of these films. The spectrum for the "3%" film is narrower, which relates to a more narrow distribution of pitch sizes.

Films were dried in larger Petri dishes, but these films tended to curve and peel off more easily, which would make it more difficult to obtain comparable UV-Vis spectra, which requires flat films. Appendix 1a shows that the spectrum is more narrow and blue-shifted for the smaller Petri dish sample, which is more desirable. Therefore, the smaller Petri dishes were used. Equation 1 states that the angle of incidence of light affects the reflected wavelength, for chiral nematic structural colour. This effect was observed for the films of this study in angle-dependent UV-Vis, presented in Appendix 1b.

4.2. Film formation through altering the evaporation temperature

This study explores the effect of drying temperature on the appearance of structural colour in the resultant films dried from CNC suspensions. The films were analysed visually and through UV-Vis spectroscopy. According to the study by Beck et al.,[5] increasing the evaporation temperature during EISA red-shifts films, while decreasing the evaporation rate blue-shifts films. Therefore, this effect should be easy to quantify using UV-Vis characterization of the films. Control of colour in dried films would be very useful, for example, in design applications and specific wavelength reflectors. The ability to control the colour simply through altering the evaporation temperature or the evaporation rate through other means would present a simple tool for producing these on a larger scale. This work attempts to uncover how applicable this simple method really is.

4.2.1. Evaporation rate

The evaporation of water was monitored as a function of drying from initial suspension state (3%) to dry film (Figure 12). The evaporation for films dried at 51 and 61 °C was not monitored, as the scale was unable to function at this high temperature. Also, the humidity was not monitored. There is a void in the results for the T28 sample due to technical problems at that specific time. Nevertheless, the results gathered after the void are reliable. The evaporation rate was near constant during the whole drying (for all samples), except for the last part of the drying, where the curves started to level horizontally. This region likely coincides with kinetic arrest,[9,55] where the suspension irreversibly gels. Table 3 lists the evaporation rates obtained with OriginPro software. The evaporation rates increase with temperature in an almost linear manner. Comparable evaporation rates have been measured before.[11,73]

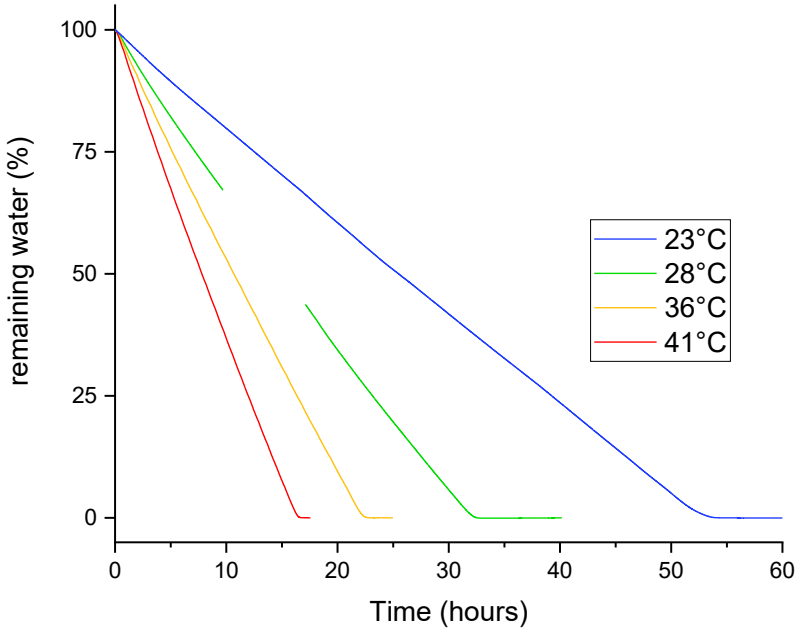

Figure 12. The remaining water as a function of time in CNC suspensions subsequently transformed into dry films at 0% remaining water. The remaining water describes the water volume lost to achieve the equilibrium water content in the film at the respective temperature.

Table 3. Evaporation rates calculated from the slope of the long linear region of the curves in Figure 12.

Sample	Evaporation rate, g/h
T23	0,071
T28	0,12
T36	0,17
T41	0,24

4.2.2. Visual observations

The films were visually observed to examine the macroscopic differences in the formation of structural colour. Figure 13 shows that the central region in each film becomes redder as the drying rate and temperature increases. Previous studies have reported red-shifts, observed visually in the centre of films dried at elevated drying rates, which were controlled through temperature[5] and pressure.[60] It appears that only the centre of the films in this study was affected by the drying temperature elevation, as the edges show a similar blue colour independent of temperature (Figure 13 d, e, f). Furthermore, there is a circular spacing visible

between the film and the Petri dish edges, when moving radially from the centre towards the edges. This spacing is thicker in films dried at higher temperatures. The evaporation rate may have been locally higher at the edges of the Petri dish, effectively resulting in a particulate motion towards the edges and upwards along the Petri dish vertical edge. This effect was likely pronounced at higher temperatures, which would explain the spacing.

In drying particulate suspensions, residual stress builds up due to capillary forces, when the drying front moves through the film from top to bottom.[71,72] This residual stress can result in cracks in dry films if it is released. Generally, the films dried at low temperatures (Figure 13 a, d) cracked more than the films dried at high temperatures (Figure 13 c, f). Therefore, the residual stress inside the lower temperature films may have been higher. Within the suspensions dried at high temperatures, the capillary forces may not have created residual stress, but instead contracted the whole film, resulting in the larger spacing. However, the films dried at higher temperature were also thicker, which could prevent the release of the residual stress into cracks. In particulate suspensions where the particles lack chiral interactions or a self-assembly capacity, it is reasonable to study the build-up of residual stress on the microscopic level, or as inter-particle interactions. In contrast, CNC suspensions form clusters of chiral nematic liquid crystalline structures with longer range order, called domains. The capillary interactions may differ considerably at inter-particle and inter-domain scales, or between particles in a liquid crystalline phase and particles in an isotropic phase. These differences are relevant since the formation of tactoids and domains may differ in CNC suspensions becoming more concentrated at different rates and at different temperatures.

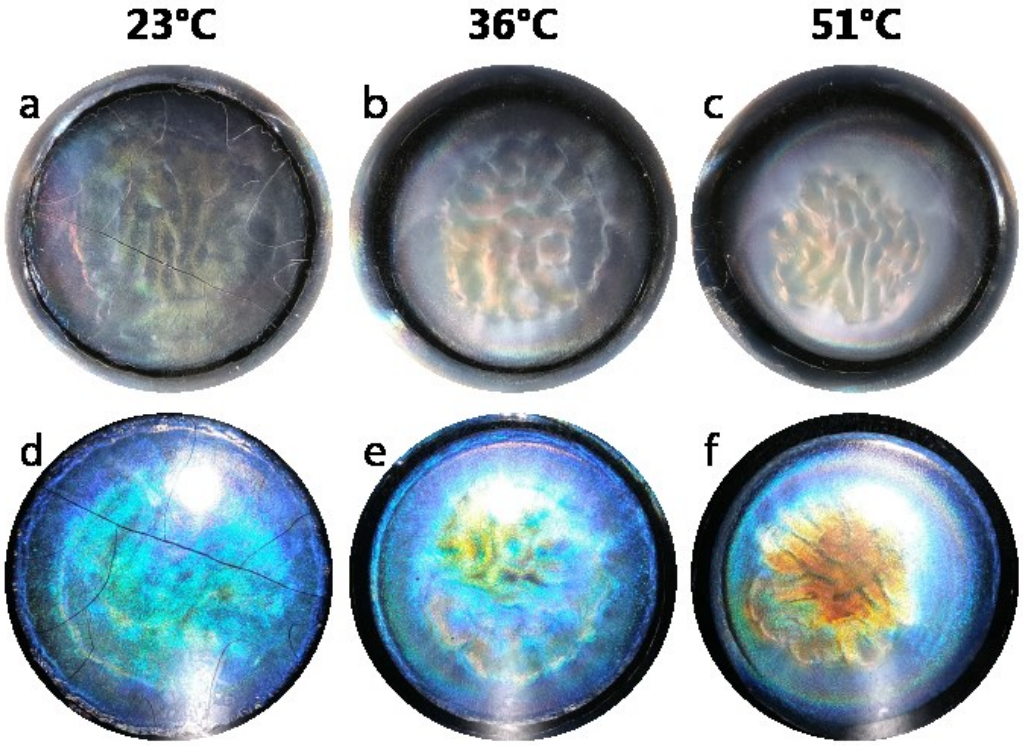

Figure 13. Photograph of three of the sample films: (a, d) T23 (b, e) T36 (c, f) T51. Photographs (d, e, f) were taken using a camera flash, in a dark environment, while photographs (a, b, c) were taken with light sources at the sides.

4.2.3. UV-Vis spectroscopy results

UV-Vis transmission spectra were obtained for each sample (Figure 14a). In order to better show the major trend, the spectra were normalized (Figure 14b), by setting all the transmission values at 374 nm to 0%. In addition, Figure 14b shows the standard deviation (from three measurements) as the coloured area around each average spectrum. T36 was omitted because it is the only sample that does not follow the trend perfectly. The T23 spectrum is narrow around the minimum transmission value, while the bandwidths become wider as the drying temperature increases. The wider spectra, especially T51 and T61, seem to be sums of several smaller spectra stitched together. In addition, the standard deviation increases as the temperature increases. The bandwidth widening suggest that there is a larger variation of colour in the high temperature films, both radially and/or through the thickness, whereas the standard deviation increase suggests that there are also increasingly circumferential colour differences. The variation in reflected colour, according to Equation 1, depends on either a difference in pitch size, or on a difference in the tilt of the chiral nematic axes, which effectively alter the viewing

angle. These differences likely play out between chiral nematic domains, which themselves contain more singular pitch sizes and axis orientations. However, it is difficult to conclude which one dominates, and without SEM images these remain speculations. Nonetheless, these results show that increasing the drying temperature essentially deteriorates the desired chiral nematic order within the films. Elevated drying rates and therefore elevated particle motion inside the drying suspension may inhibit, to some degree, the self-assembly of the CNCs into long-range order formations. In previous work, similar results have been shown. Red-shifts and bandwidth broadening in transmission spectra has been observed by elevating the drying rate by altering the temperature[5] and pressure[60]. The same has been shown also in reflectance spectra, by directly altering the evaporation rate in controlled temperature, pressure and humidity conditions.[73] The standard deviation for spectra, however, has not been present in previous studies.

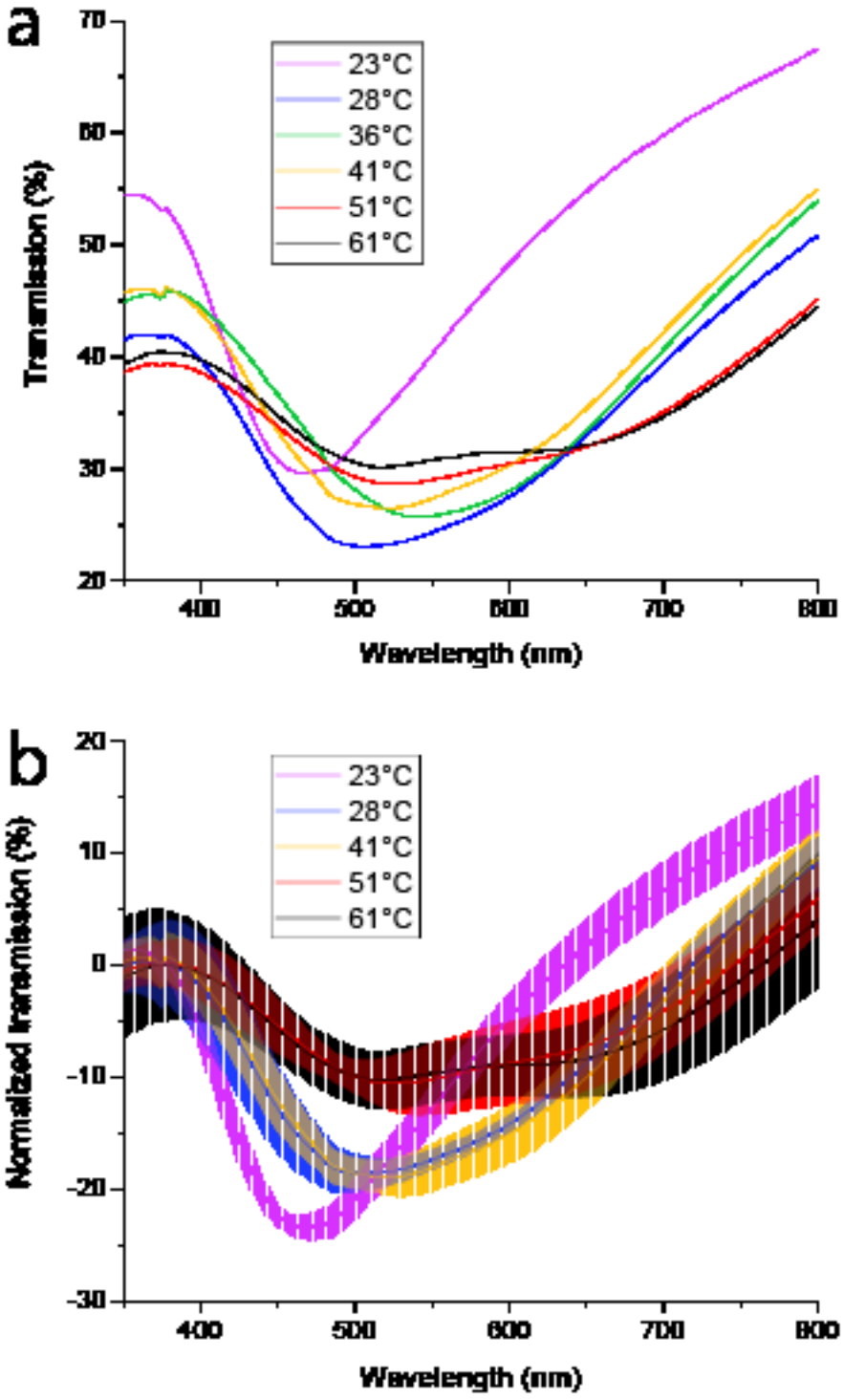

Figure 14. UV-Vis spectroscopy spectra of all the samples in this study. (a) Unmodified average transmission spectra of three measurement points. (b) The same transmission spectra (except for T36), but the transmission value at 374 nm normalized to 0%. The coloured area illustrates the standard deviation for every average transmission value.

4.3. Film formation through altering the initial concentration

This section explores the film-forming behaviour further, by investigating the effect of the initial concentration used in EISA. The drying temperature, on the other hand, was kept constant at room temperature, because this temperature produced the best films, as discussed in section 4.2. The previous sections also showed that the production of films with a more uniform distribution of structural colour was challenging. Altering the initial conditions prior to EISA could produce solid films with a more even and defined helical order.

When a suspension of nanocrystals is drying, the concentration, as well as the anisotropic volume fraction, increases over time.[13,36] The pitch decreases, and domains form and coalesce until the crystals solidify into a dry film.[57] These concentration dependent effects exist independent of the initial concentration of the CNC suspension. In other words, all drying suspensions pass the same concentration regimes responsible for the self-assembly behaviour. Therefore, it could be inferred that the initial concentration should not affect the colour properties of the dried films. However, this assumption presumes that the concentration-dependent self-assembly is instant. If the self-assembly is time-dependent, suspensions dried from below w_0 and from above w_0 should give different film structures, if only slightly. Suspensions initially in the isotropic regime will not have time to self-assemble to the same extent as suspensions having been in the anisotropic concentration regime for a much longer time than the evaporation time. This study attempted to uncover the extent of the difference. Shear forces applied during pipetting of the suspension may completely reverse the chiral nematic ordering.[63] Therefore, it is important to give the sample time to equilibrate, without evaporation or external forces, inside the container in which the EISA happens, in order to investigate the effect of initial concentration at equilibrium conditions. Sections 4.3.3., 4.3.4. and 4.3.5. provide results of commonly used analysis tools, while section 4.3.6. discusses these results and correlates them with a structural analysis provided by SEM.

4.3.1. Anisotropic volume fraction in CNC suspensions

The concentration-dependent AVF is a good approximate measure of the extent of self-assembly in a liquid crystalline suspension, i.e. the fraction of nanocrystals existing in a liquid crystalline order.[4] Therefore, the initial AVF was used for choosing the initial concentrations in

this study. Figure 15 shows a phase separated CNC suspension where the phase boundary is clearly visible. Figure 15 also displays the AVF, measured from the relative height of the AVF to the total liquid height, as a function of concentration, after one, five and 14 weeks of stabilization in the vials. Phase separation occurs somewhere between 3 and 4 percent for CNC used in this study. In the 4, 5, 6 and 7% CNC suspensions there is a clearly visible phase boundary, while the 3% suspension seems to be completely isotropic. Honorato-Rios et al.[13] also found a w_0 value between 3 and 4%, and a less clear phase boundary at the high AVF at 9%. The 7% suspension might have 3 phases, as was hypothesized by Honorato-Rios et al.[13] for their 9% sample. Higher critical w_0 values have been recorded,[29,36,53] likely due to differing CNC aspect ratios or surface charges.[29]

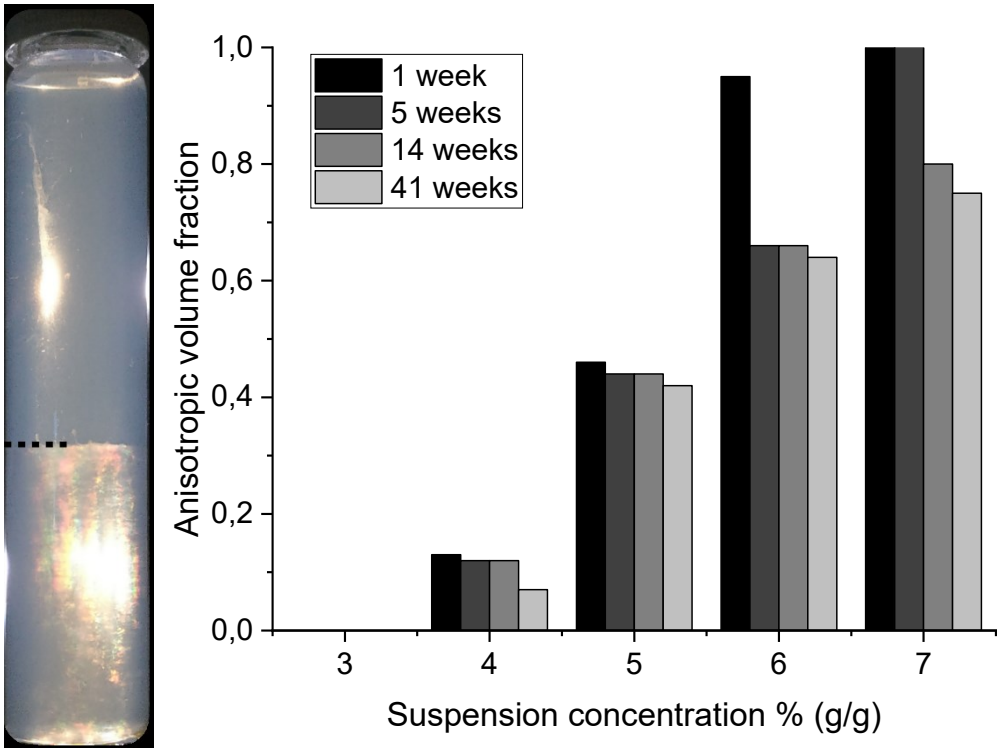

Figure 15. To the left a 5% CNC suspensions after 14 weeks undisturbed. The dashed black line indicates the position of the phase boundary between the upper isotropic and the lower anisotropic phase. To the right anisotropic volume fraction as a function of CNC suspension concentration (w/w), at different observation times.

4.3.2. Substrate treatment

Petri dishes were treated to decrease the contact angle and improve the interaction between the substrate and CNC suspension. Table 4 displays the water contact angles on the pristine and

treated Petri dishes. The treated substrates are considerably more hydrophilic, although there is not a large difference between the two treated Petri dishes.

Table 4. Contact angles on different substrates.

Substrate	**Static contact angle**
Untreated Petri dish	87.6°
Treated (ozone/water) Petri dish	42.4°
Treated (ozone/ethanol) Petri dish	40.0°

Figure 16 shows a film assembled in untreated Petri dish (Figure 16a), and in a Petri dish treated with ozone and ethanol (Figure 16b). The most notable difference is the circular crack near the edge in the left sample. While the large black area in the sample dried in the hydrophilized Petri dish might look like a crack, it is in fact a thinner transparent area. The higher affinity of the hydrophilic nanocrystals towards the treated substrate explains the continuity of the right film in Figure 16b. Although the structure in the central area of the films look slightly different, the colour is almost the same, which the UV-Vis spectra confirm in Figure 16c. However, the spectrum for the treated substrate film has a narrower bandwidth than the pristine substrate film, indicating a narrower distribution of pitches in the treated substrate film.

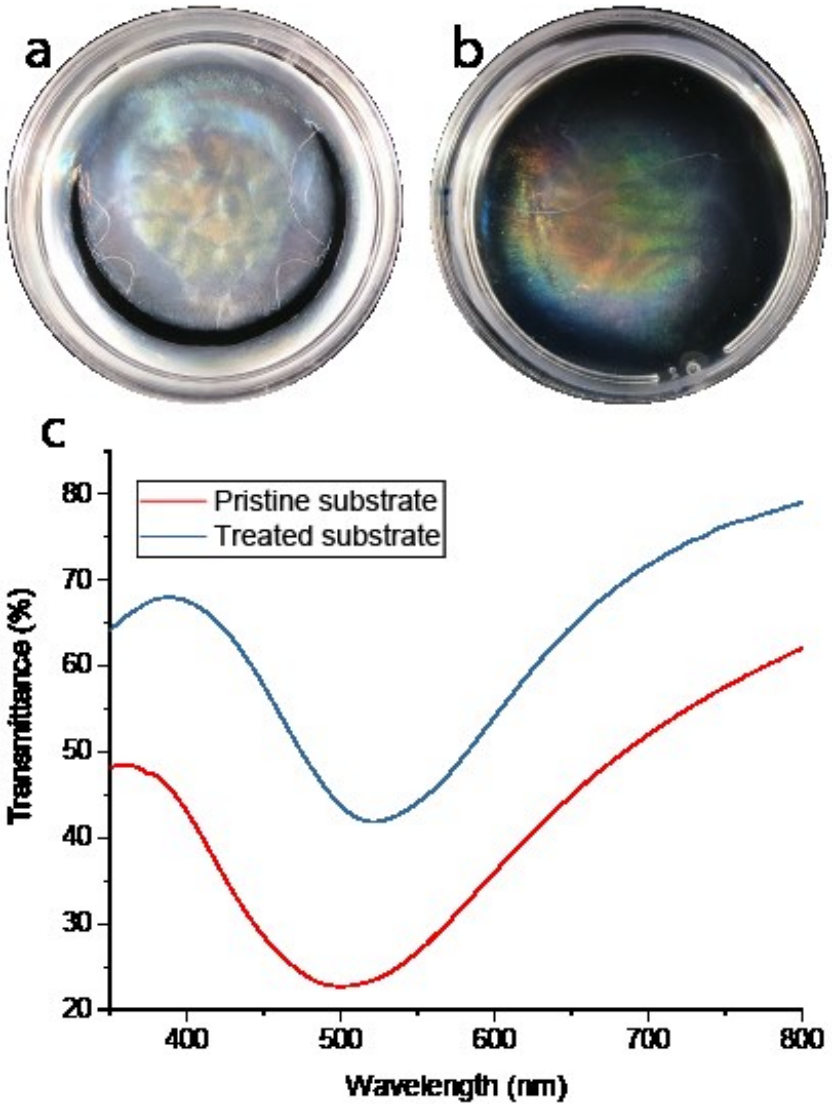

Figure 16. Sample films assembled at the same conditions, but on different substrates: (a) An untreated Petri dish, (b) a Petri dish treated with ozone and water. (c) UV-Vis Transmission spectra of the films.

Nguyen et al.[16] studied the effect of substrate on EISA, but didn't find any clear correlation between the substrate polarity and film colour, although different substrates yielded very varied colours, indicating the importance of the surface chemical composition rather than the polarity. However, very hydrophobic substrates produced less colourful opaque films. Based on Figure 16, the treatment affects the reflected colour only to a small extent.

4.3.3. Film casting and visual observations

Films were dried from the same stock suspension, but at different starting concentrations, diluted from the stock suspension. The 3, 4, 5, 6 and 7% starting concentrations were chosen for the film casting, based on the data in Figure 15. The suspensions were cast and dried in Petri dishes treated with ozone/ethanol (NE_e3, NE_e4, NE_e5, NE_e6, NE_e7) and ozone/water (NE_w3, NE_w4, NE_w5, NE_w6, NE_w7). A parallel range of samples were equilibrated prior to drying by isolating the Petri dishes with a lids after casting, in order to allow the suspensions to relax from the shear forces caused by the pipetting. Suspensions cast in Petri dishes treated with ozone/ethanol were equilibrated for three days (E_e3, E_e4, E_e5, E_e6, E_e7), while the suspensions cast in Petri dishes treated with ozone/water were equilibrated for seven days (E_w3, E_w4, E_w5, E_w6, E_w7). All films contained an equal total solids mass of 120 mg and were dried in 21°C and a low humidity of 20%, to ensure a relatively fast drying.[6] Therefore, differences in film thickness result from either radial thickness gradients or packing density differences. The low humidity was chosen to limit the extent of self-assembly during the post-w_0 and pre-w_k stage of the drying, and thus enhance the self-assembly contribution during equilibration. Since the initial suspension volume decreased with increasing concentration, the drying time decreased.

Figure 17 displays photographs of all the films of this study, taken from the bottom side of the film, though the transparent Petri dish substrate, and against a black background. The structural colour colour in the films is generated by the selective reflection of left-handed circularly polarized light, in accordance with Equation 1.[35] In General, drying droplets of CNC suspensions form films, which red-shift towards the film edges in a radial manner,[7,62] because of the coffee-ring effect.[62] However, the films in this work films assembled in Petri dishes have a red-shifted centre, which has been observed earlier for films dried in Petri dishes.[11,14] Whereas the low initial concentration samples completely cover the Petri dish surface, the higher concentration samples contain a circular or moon shaped crack, or discontinuity, towards the Petri dish edge, which increases with size for higher concentration films. This effect is might be caused by residual stress building up during the drying, which would increase for higher initial concentration samples.

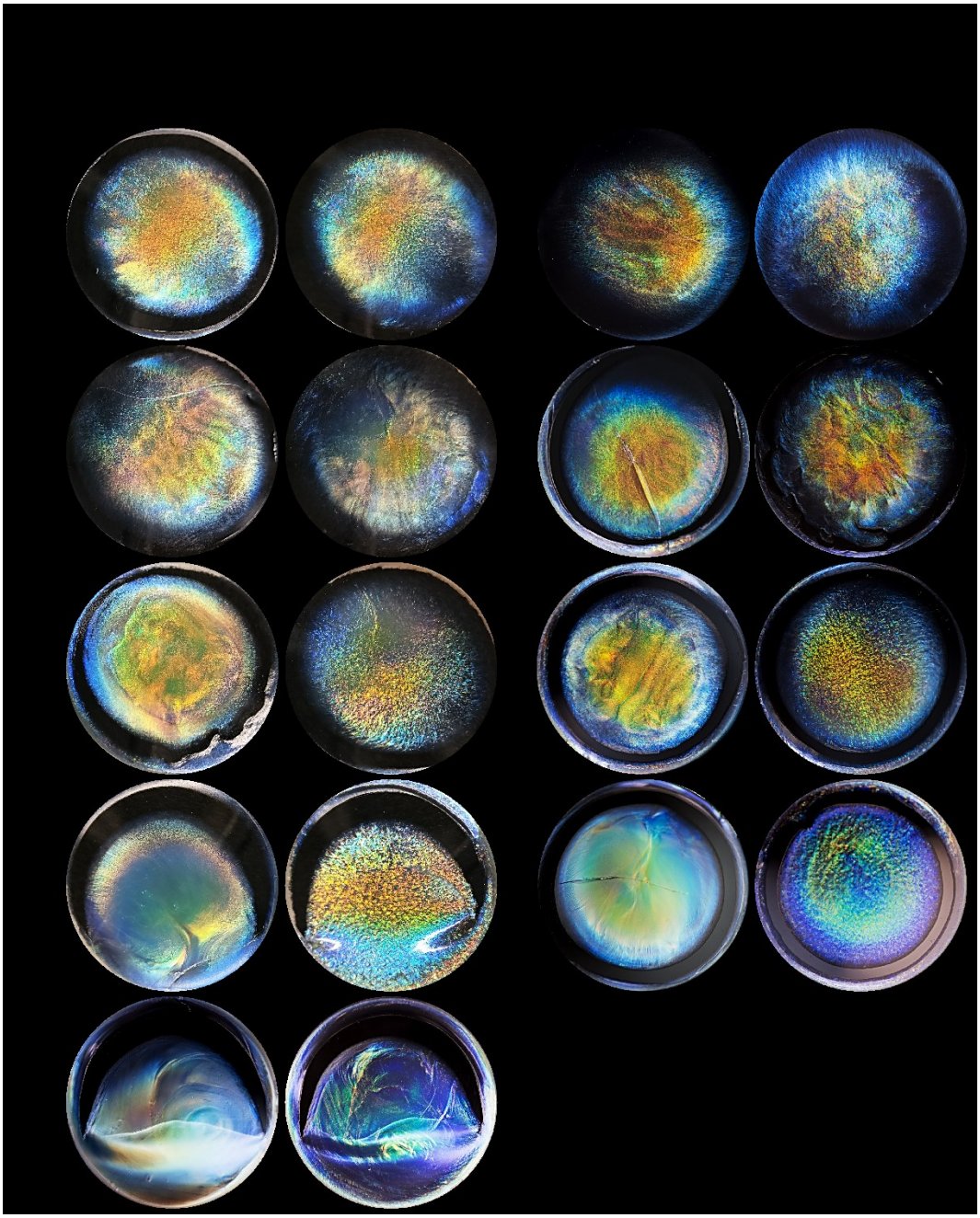

Figure 17. Photographs of the sample films, taken against a black background. The difference between equilibration and non-equilibration is pronounced for the samples dried from higher concentrations.

Figure 17 shows the considerable effect of initial concentration on the dried films. Furthermore, the effect of equilibration becomes apparent when moving towards the higher initial concentration films. In addition, the equilibration only affects the structural colour of the films, while the shape remains unchanged by the equilibration. The lack of an AVF in the 3% suspension explains the negligible difference between the 3% samples. Equilibration has a very

little effect on a suspension in the fully isotropic regime, which contains no liquid crystalline tactoids.[57] In contrast, the suspensions containing a high initial AVF require equilibration to fully develop their structural colour generating capacity. This is especially apparent in the 7% samples, where the equilibrated film displays a deeper and clearer blue colour and the non-equilibrated film a more opaque colour.

Next, Figure 17 further demonstrates the difference, and more importantly, the similarities, between the two parallel sample sets (column 1 and 2 versus 3 and 4), where only the substrate and equilibration time (3 versus 7) was varied. The trends mentioned above are clearly confirmed by both sample sets. Equilibration times longer than 3 days are likely redundant. However, the films cast on the substrates treated with ozone/ethanol are more centred, which is clearly visible when comparing the 6% films in the different sets. The different surface chemistry and the lower contact angle (Table 4) probably enhances the interaction of the nanocrystals to ozone/ethanol treated substrate.

The effect of initial concentration on the formation of reflective materials from CNCs has been briefly overviewed before, at lower concentration ranges (0.6-3.7%)[17] and with AVFs of 0 and close to 100%.[14] Tran et al.[11] examined the effect of equilibration time for a 4.2% CNC suspension, where the AVF should be close to 0 according to Figure 15. However, it is important to note that w_0 and the evolution of the AVF highly depends on the inherent CNC properties, mainly the aspect ratio and charge, effectively making any comparison only approximate.[13,29,46] This work attempts to thoroughly gain insight into the effects of the initial AVF and equilibration, by further analysing the samples in UV-Vis spectroscopy, optical microscopy and SEM.

4.3.4. UV-Vis spectroscopy results

UV-Vis spectroscopy provides information on the average pitch size of the ordered regions in films assembled from cellulose nanocrystal suspensions. Figure 18 shows UV-Vis transmission spectra, measured from all the 18 sample films in this study. The spectra are averages calculated from three spectra, measured in the central area of the film at an equal radial distance from the centre of the films. The minimum transmission in the graphs corresponds with the maximum in reflection. In several of the graphs, showing the difference between non-equilibrated and equilibrated films, the equilibration results in a blue-shift of the maximum reflection

wavelength, i. e. the blue curve is shifted towards the left. This blue-shift in equilibrated films is in line with the work of Tran et al.[11] There are, however, some inconsistencies to this trend, especially clear in the 6% films in the left row of Figure 18. Nonetheless, there is another, more important trend worth stressing. The difference in spectral width, close to the minimum wavelength, consistently increases with concentration. The films prepared from equilibrated suspensions at high initial AVF have narrower spectral bandwidths because of a narrower distribution of pitch sizes in these films.

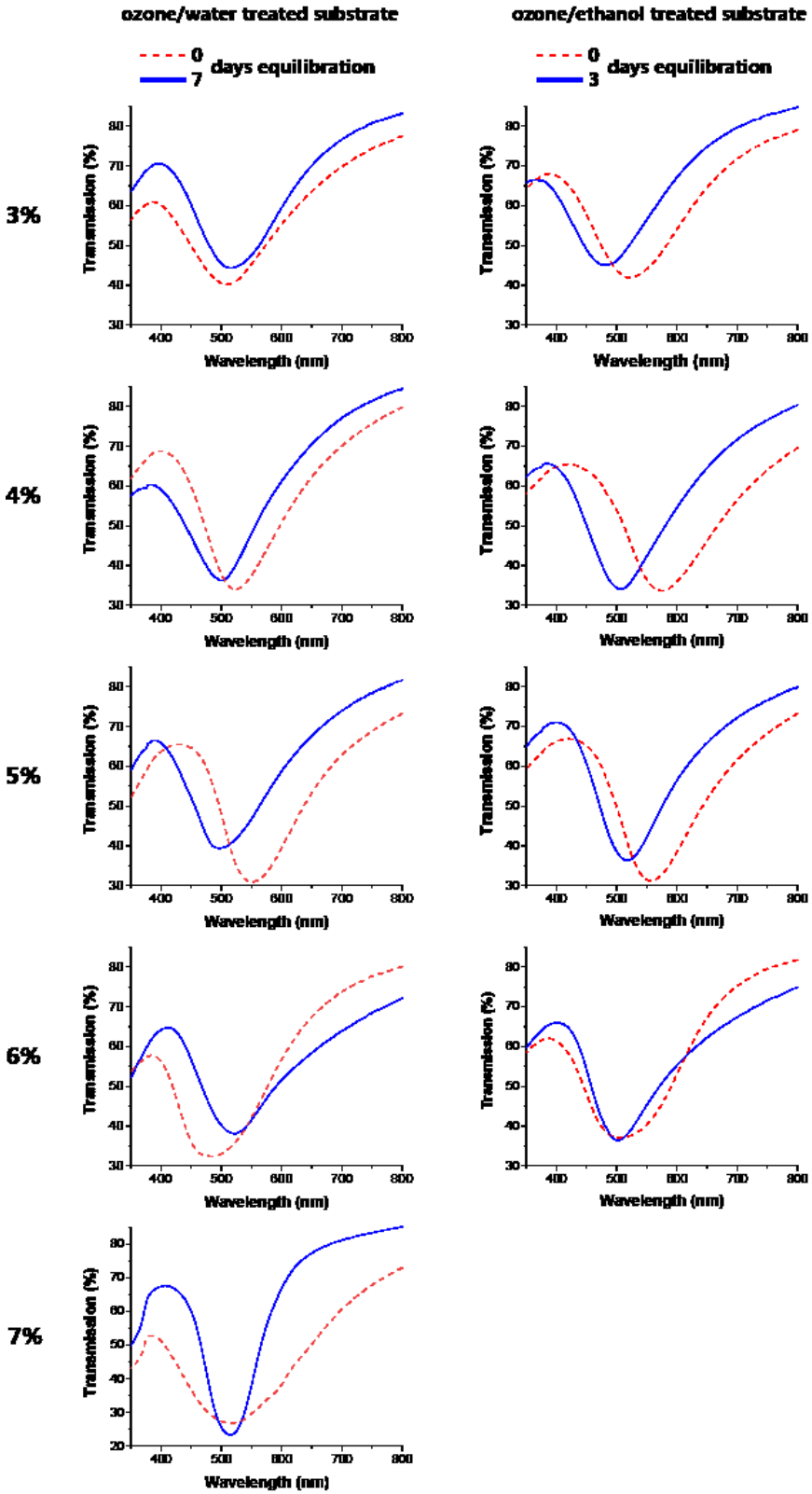

Figure 18. UV-Vis transmission spectra of the films in this study, as averages of three points measured at the central region of the film and at equal distances from the centre. The equilibrated spectra are narrower at high concentration.

4.3.5. Optical microscopy results

Optical microscopy reveals the structure of the colour in chiral nematic CNC films, thereby providing insight into the architecture of the chiral nematic domains, which are the elemental units with uniform pitch and chiral nematic axis orientation. Figure 19 shows micrographs of the 10 films assembled on Petri dishes hydrophilized with ozone/water. Each area with uniform colour corresponds to a domain.[8] The variation in colour is caused by either a difference in pitch size, or by a tilt in CNCs from the film plane, according to Equation 1.[35] The films contain smaller domains as the concentration increases for the non-equilibrated samples, and larger uniform domains as the concentration increases for the equilibrated samples. The longer evaporation time for the NE_w3 film results in larger uniform domains, whereas smaller domains are visible in the NE_w6, with a shorter drying time. This stems from the earlier kinetic arrest[9,55] for the 6% suspension upon drying, preventing long-range ordered domains to form during the shorter time. Equilibration prior to drying allowed the suspensions to relax from the mixing caused by pipetting upon casting. Equilibration was expected to be essential especially for the higher AVF samples, where phase separation takes longer (Figure 15). This explains the large domains visible in the equilibrated and high concentration samples.

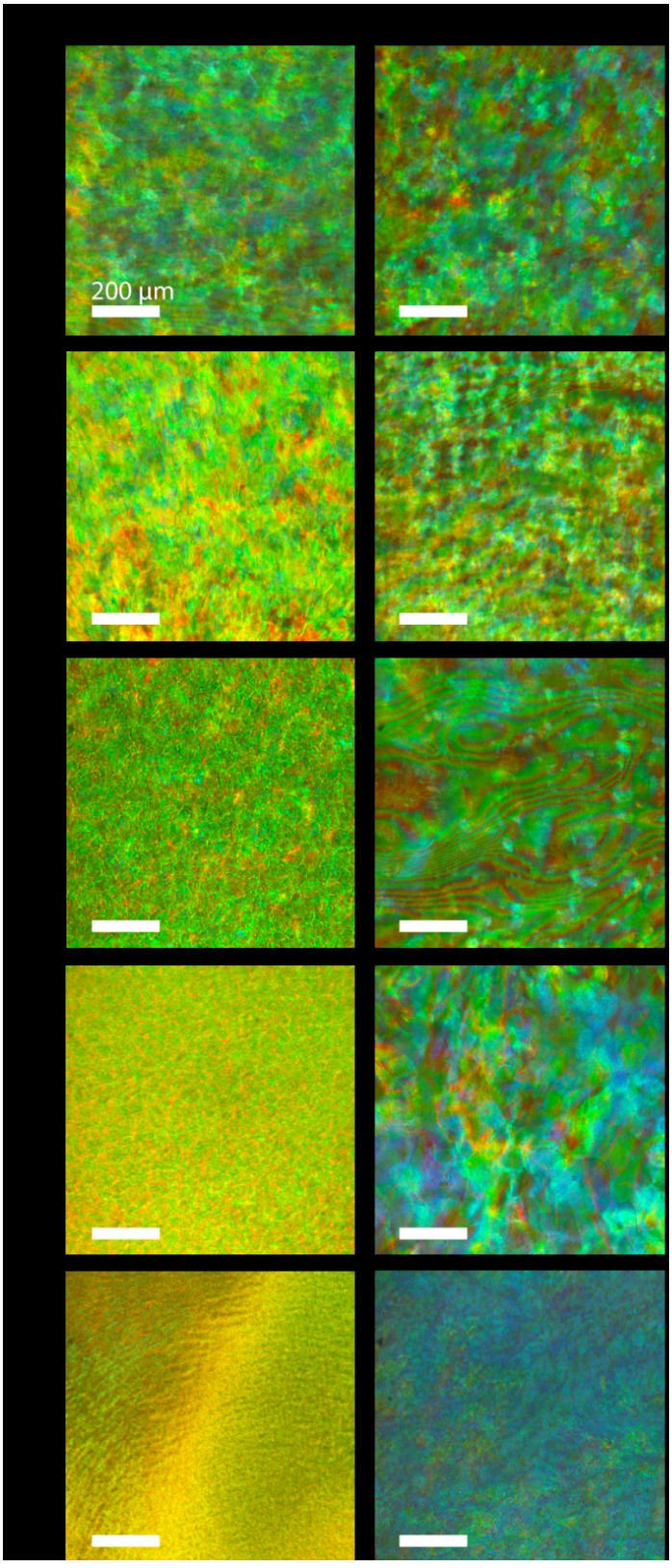

Figure 19. Microscope images of all the films assembled in Petri dishes treated with water/ozone. The difference between equilibration and non-equilibration is pronounced for the samples dried from higher concentrations.

4.3.6. Discussion and scanning electron microscopy results

The microscopy images in Figure 19 and the film photographs in Figure 17 both suggest that equilibration becomes increasingly important when the initial concentration is higher, whereas it is negligible when there is no anisotropic phase. Consequently, the equilibration mainly acts on the AVF. At the critical concentration, the AVF only contains small tactoids[57] that merge and become larger domains as the concentration increases. These long-range transitions are likely time-dependent as well as concentration-dependent. Films formed from suspensions at low concentrations of CNCs[5,15,48,49,60] show reductions in the specific reflection of structural colours because the suspension exists in the post-critical concentration and pre-gelation state for too short times. Thus, the drying time should limit the amount and size of domains forming in suspensions without domains prior to the evaporation. Lowering the evaporation rate[5,60] addresses this, but the evaporation-induced particulate motion[17,74] inside the suspension may still hinder the formation to a greater extent than in a suspension at equilibrium. Films have previously been assembled from suspensions at high AVF,[14,63] which already contain the domains that create the structural colour. However, when the CNC suspension is transferred to the substrate for solvent casting using a pipette, the resultant mixing disrupts the chiral nematic order in the suspension. Gray & Mu[63] discovered that weak shear forces applied to a high concentration (9.6%) suspension of CNCs untwists the chiral nematic order. Nematic-like textures were observed in a microscope for a sample squeezed between microscope glasses. They subsequently observed a relaxation transition from nematically to chiral nematically ordered nanocrystals in the 9,6% CNC suspension, during 18 hours. Similar phenomena might be present at suspension transfer into Petri dishes, especially at high AVF, where the viscosity is significantly higher.[56,63,74]

SEM images obtained from the films described in Figure 17 provided further insight into the chiral nematic pitch distribution differences with the films as a function of processing steps (Figure 20). The images are from cross-sections of the films fractured at the centre, which usually has the highest ordering[8,58]. The middle column (Figure 20 b, e, h) shows SEM images of the cross section of the E_w3, NE_w6 and E_w6 samples, whereas the left (Figure 20 a, d, g) and right (Figure 20 c, f, i) columns shows high magnification images of the respective top and bottom parts of the cross sections. The top row (Figure 20 a, b, c) displays images of the E_w3 sample, which is also a good reference that is comparable with studies where films were assembled from

low concentration suspensions.[5,15,48,49,60] As described in Figure 19 and Figure 18, the effect of equilibration on the E_w3 sample was not significant and therefore the cross section images of this sample are complemented with both 6% samples, NE_w6 (Figure 20 d, e, f) and E_w6 (Figure 20 g, h, i), where the effect of equilibration is most evident.

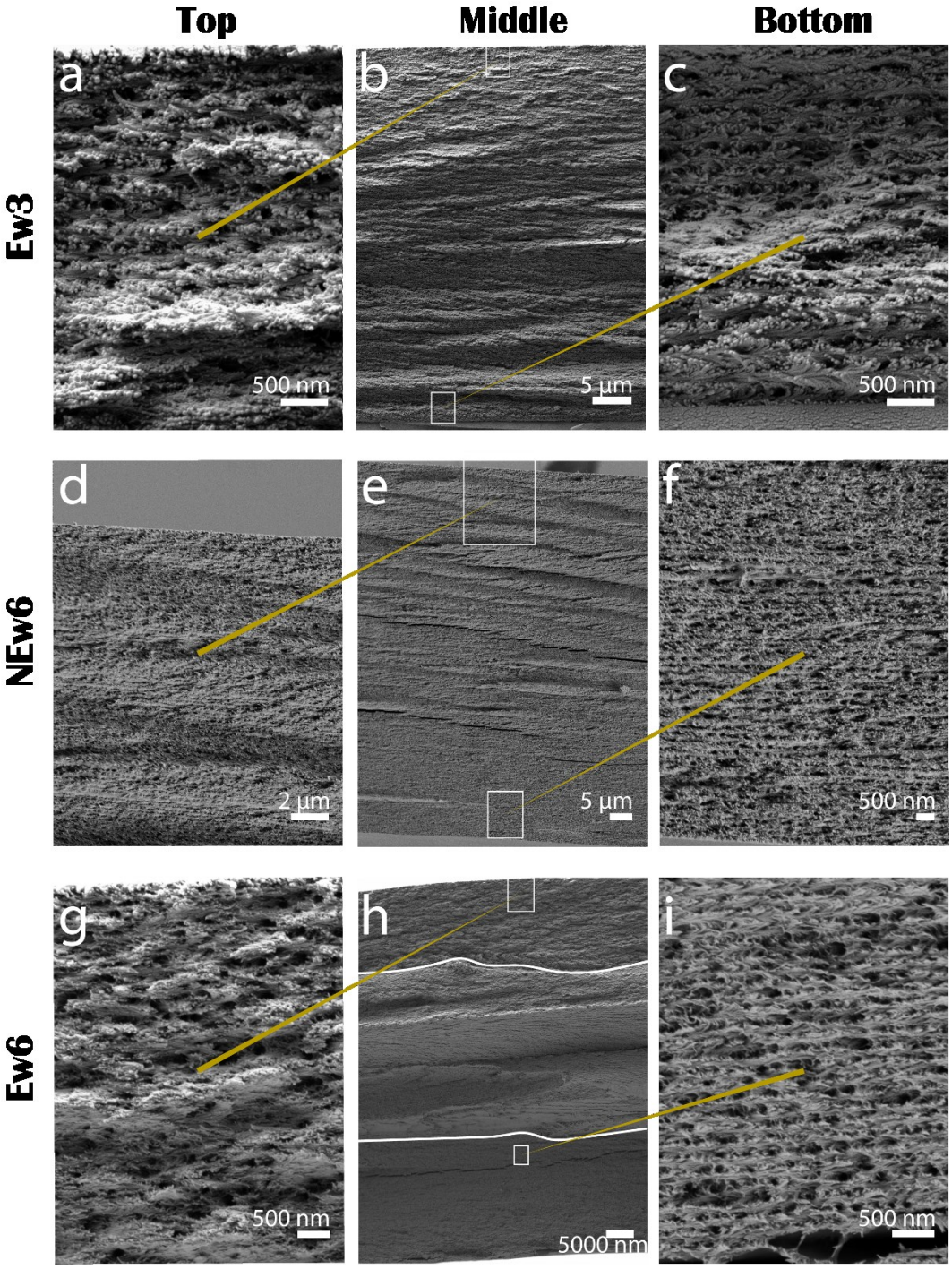

Figure 20. SEM images of the (a-c) E_w3 film, (d-e) NE_w6 film, and (g-h) E_w6 film. (b, e, h) Cross-sections through the whole thickness of the film, at the radial centre of the film. (a, d, g)

Zoomed-in images of the top part of the central column images, where the white boxes represent the area that was used. (c, f, i) Zoomed-in images of the bottom parts.

Considering the central column images, the E_w6 cross section (Figure 20h) has three distinct horizontal segments of stratified nanocrystals while the E_w3 (Figure 20b) and NE_w6 (Figure 20e) cross-sections are more continuous on the vertical axis. The cross sections of the NE_w6 and E_w6 samples have a cleaner and sharper fracture line than the E_w3 sample. However, the middle segment of the E_w6 cross-section does not have a sharp fracture surface. The presence of large and potentially merging tactoids led to large domains that could have caused such a discontinuity in the section which was fractured. The existence of an AVF in the 6% suspensions prior to the EISA led to better and more homogeneous helix structure with smaller pitches in the E_w6 and NE_w6 films, effectively making the surface of the fracture smoother.

The distinct chiral nematic structure is apparent in the SEM images with high magnification for the bottom section of the samples (Figure 20 c, f, i). The E_w6 film is the most ordered with the lowest pitch value, while the E_w3 film has a higher pitch (Table 5). In addition, there is a larger scatter of pitch values for the NE_w6 sample (140 nm) than the E_w6 sample (30 nm). Therefore, EISA starting from higher concentrations gives rise to lower pitch values in dried films in case the sample was equilibrated. The high pitch value for the NE_w6 film is likely caused by an early gelation during EISA. The scatter of pitch values can also be caused by a higher CNC polydispersity, where different sizes result in different pitch values. The E_w6 sample has a more narrow pitch size distribution due to a more uniform size distribution of nanocrystals in each layer. These CNCs in the bottom layer are likely of the larger fraction, which correspond with the anisotropic volume fraction of the starting suspension.

According to film height data obtained from SEM images and presented in Table 5, the thickness of E_w6 is slightly lower at 70 µm than NE_w6 at 82 µm. The E_w6 is expected to be more compressed due to the more ordered structure and lower pitch. E_w3 is much thinner than the 6% samples, at 47 µm. The coffee-ring effect[17,62] could affect the E_w3 sample more strongly than the 6% samples because the relatively longer drying time, and cause a more extensive radial height variation.

Table 5. Thickness and pitch sizes of the three samples in the study. The thicknesses are obtained from SEM images, and the pitch sizes from six measurement points from SEM images.

Sample	Thickness, µm	average pitch size in the bottom part of the film, nm
E_w3	47	395
NE_w6	82	440 ± 140
E_w6	70	330 ± 30

While the E_w3, E_w6 and NE_w6 samples all show chiral nematic order in the bottom of the films, there are differences within the samples for the top parts of the films (Figure 20 a, d, g), facing the air interface. Generally, the upper parts of CNC films are less ordered than their bottom counterparts. The surface of the suspension volume dries faster, which causes an earlier gelation.[9,55,74] The top layer forms a more disordered layer,[7,17,42] whereas the bottom segment, towards the substrate, is more ordered, where the drying is slower and the chiral nematic axis aligns vertically.[14,57] This shift from order to disorder is seen in the E_w3 film (Figure 20b) and corresponds well with previous reports.[7,14] Figure 20a shows a highly disordered and deformed helical order, while the bottom layer (Figure 20c) has a very ordered and homogeneous chiral nematic order. This layer difference is even greater in the E_w6 film. Tactoids form in the very late stage of EISA in the isotropic volume fraction, which prevents the generation of longer range order inside the top segment of the E_w6 film (Figure 20g). In addition, the E_w6 film has a clear segmented and discontinuous structure (Figure 20h), with uniformly disordered and ordered top and bottom segments, respectively. Appendix 2 shows that the middle segment (Figure 20h) is ordered but that the fracture is discontinuous. This segmented structure is distinctly different from the continuous change from order to disorder in the E_w3 film (Figure 20a-c). The thickness ratio of the disordered and ordered regions in Figure 20h approximately corresponds to the isotropic/anisotropic volume fraction ratio in suspension (Figure 15), although the fraction of order in the film is higher than the AVF in the suspension. Consequently, it can be inferred that the ordered region in Figure 20i forms from the anisotropic phase, while the disordered region in Figure 20g forms from the isotropic phase. Additionally, the isotropic phase of the E_w6 suspension contributes to both the upper disordered region in the film, and to part of the middle-ordered region where the CNCs are forming tactoids at an intermediate stage. In contrast, the NE_w6 sample contained an almost fully ordered structure through its thickness, but

with larger pitches in the bottom region (Figure 20f, Table 5), which resulted from mixing of the isotropic and anisotropic phases.

This section provides further insights and discussions into differences in long-range order in the E_w6 and NE_w6 films. Schematics provide illustrations of the formation of chiral nematic domains and the segmented structure of the films as a function of the initial equilibration state before the EISA. The elegant work of Wang *et al.*[57] showed how tactoids form and grow from an initially 4.1% CNC suspension. The tactoids grow and eventually coalesce to generate large chiral nematic domains that subsequently flatten into ellipsoids or spheroids. Figure 21a shows a sequence of SEM images of the E_w6 film, where the coloured dotted lines point out the chiral nematic domains resulting from partially merged tactoids without long-range ordered alignment in the chiral nematic matrix that surrounds them. Appendix 2 reveals that the domains contain the chiral nematic order. The planar dimensionalities of these elliptically shaped domains fits with the dimensions of the coloured spots in the corresponding microscope image inset of the E_w6 film (Figure 21a). Each domain has a specific orientation and pitch value, which reflects light according to Equation 1. However, the pitch and orientation vary in each domain, which leads to the appearance of a mosaic of colours in the Figure 21a inset. Dumanli *et al.*[8] proposed an explanation to the colour mosaic in the CNC size distribution between the domains. This is likely true for the domains in the films in this study, due to the large variation in size presented in Figure 19. The highly ordered bottom layer of the E_w6 film (Figure 20i) provides the background colour of the microscope image (Figure 2b).

Figure 21c-f propose schematics for the evolution of chiral nematic structures during drying, in the central part of the film, where the meniscus is assumed macroscopically horizontal. Figure 21c displays the condition of the suspension after equilibration for 7 days. The blue sheets correspond to the layered helical order within the anisotropic volume fraction of the phase separated CNC suspension, where each sheet represent a 180° rotation of the chiral nematic director. Wang *et al.*[57] observed that most of the anisotropic phase forms a continuous lamellar structure in suspension, where the chiral nematic axis is perpendicular to the substrate plane. The globes represent spherical chiral nematic domains in the isotropic phase, with chiral nematic axes that are randomly oriented. When the drying starts, following the route Figure 21c → d, the domains align on top of the continuous lamellar phase, and subsequently flatten. Tactoids observed in suspensions[4] and captured in resins from suspensions[57] are spherical in nature.

However, the domains in Figure 21a are distinctly ellipsoidal in shape. These were likely flattened by anisotropic shrinkage or packing[57] during assembly. This is supported by the fact that considerably larger pitches have been observed in the liquid state for CNC suspensions than in the dry state for CNC films. Appendix 2 further highlights the elliptical or disc shaped geometry of the E_w6 sample domains. Wang *et al.*[57] observed that domains formed from a CNC suspension where the chiral nematic axes were aligned with both the long and short axes of the elliptical domain. In thet films assembled here, the chiral nematic axis is only parallell with the short axis. There is no evidence for whether the spherical domains first become elliptical and then align when they start to settle, or whether the spherical domains first start to settle, orient, and subsequently get more elliptical in shape due to packing.

The less ordered non-helical part of the isotropic volume fraction forms a thick disordered top part of the film, presented by the randomly oriented CNCs in Figure 21d. The equilibration ensured there was time for the more ordered chiral nematic phase to form at the bottom of the suspension. The resultant film has a segmented structure, observed in Figure 20h, with the continuous lamellar structure in the bottom, larger elliptical and ordered domains in the central segment, and a highly disordered structure in the top segment.

The SEM image of the NE_w6 film in Figure 21b portrays a very different structure. The more continuous structure produces smaller elliptically shaped formations in the upper half of the film, pointed out by the yellow dotted lines. The formations are smaller and less apparent than the elliptical formations in the E_w6 film (Figure 21a). The colour structure of the microscope image inset in Figure 21b matches with the film cross-section structure, where the smaller chiral nematic domains induces a colour mosaic with smaller colour areas. Dumanli et al.[8] observed domains in solid films with dimensions of 2 to 20 µm, the sizes of which are more comparable with the domains in the NE_w6 film (Figure 21b) than those in the E_w6 film. Lack of equilibration and a lower starting concentration (4,1%) likely limited the size of the domains in the film by Dumanli et al.[8]

Figure 21e-f displays schematically the hypothesized EISA of a non-equilibrated 6% suspension. The transfer of a suspension at equilibrium (Figure 21e) into a Petri dish by the means of a pipette induces shearing and thus mixing into the suspension from the flow through the tip. The chiral nematic liquid crystal arrangement is unwound into a more nematic-like

order[63] (Figure 21f). Chen & Gray[75] obtained the interfacial tension at the isotropic/anisotropic phase boundary, and they obtained values that varied from $1.9*10^{-4}$ to $8.3*10^{-4}$ mN m^{-1}, which are considerably low. In addition, the interfacial tension increased as the concentration increased. Thus, the anisotropic and isotropic phases may become very interdigitated, even under the effect of weak shearing forces, which could disrupt the long-range continuity. The sample starts drying in a non-equilibrium, disordered condition, following Figure 21e → f. Drying starts immediately after casting and the sample enters the gelled and glassy state[9] close after the casting. Figure 15 shows that phase separation is slow for high concentration (6%) samples. The chiral nematic domains do not re-establish their original size during the short drying time and the disorder remains in the assembled film.

The resultant film has a higher pitch size and pitch size variation (Table 5). Many samples in the literature[7-9,14,17,20,62] have been assembled from an initial suspension concentration above 4%, where an anisotropic phase is likely present. These films were likely formed from a suspension in a non-equilibrated state, according to Figure 21 route e → f. This effectively limits the formation of ordered helical structures, and therefore prevents the full structural colour potential.

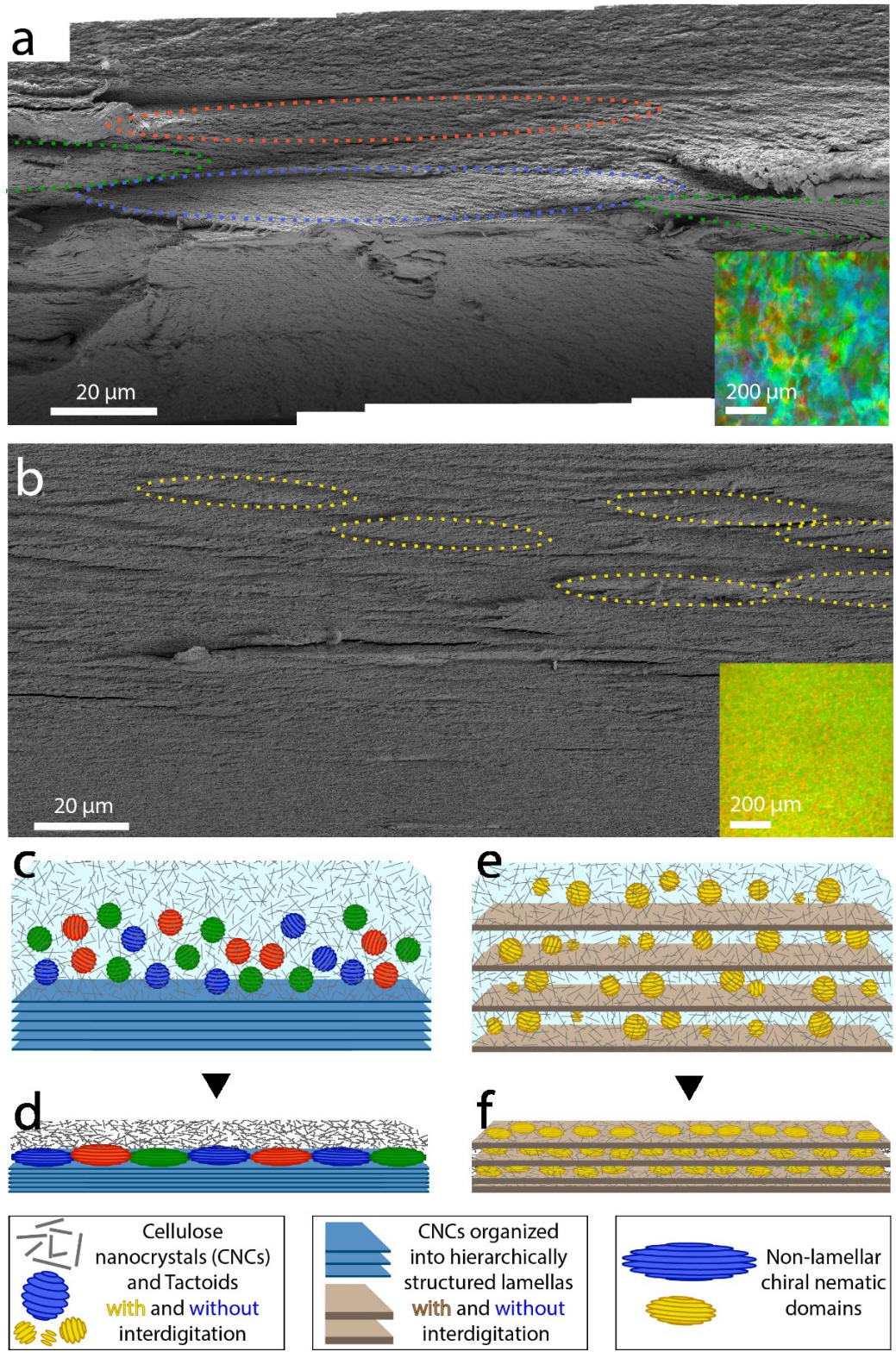

Figure 21. SEM images of (a) E_w6 and (b) NE_w6, showing the cross-sections through the whole thickness of the films, at the radial centre of the films. The dotted areas indicate domains, and the insets are microscope images of the corresponding sample films. (c-f) Schematic illustrations showing the chiral nematic formations (c, e) before, and (d, f) after EISA, for the (c, d) E_w6, and (e, f) NE_w6 sample films.

5. CONCLUSIONS

This work examined in detail the formation of colour-generating helical order in dry CNC films, as a function of the conditions prior to and during the evaporation-induced self-assembly procedure. This was done through two separate studies, examining the drying temperature and the initial concentration, as well as through initial work performed to find the right parameters.

Evaporation-induced self-assembly (EISA) at elevated temperatures (23 → 61 °C) resulted in films with increasingly red-shifted centres and radial colour variation. Furthermore, the films were more contracted radially towards the centre, but cracked less than their low temperature dried counterparts. UV-Vis spectroscopy revealed greater distributions of pitch sizes and/or chiral nematic domain axes orientations in films dried at elevated temperatures. Industrial production of CNC surfaces would enjoy faster EISA in order to produce films more cost-efficiently. However, as shown in this study, higher evaporation rates limit the full potential of the development of structural colour in CNC films.

The second study was related the appearance of helical order in dry films as a function of the starting concentration, and thus, anisotropic volume fraction (AVF) in cellulose nanocrystal suspensions. The AVF increased as a function of concentration and decreased as a function of time. The combination of high initial AVF and equilibration prior to EISA promoted the formation of ordered chiral nematic structures and large merged domains, as was demonstrated by UV-Vis spectroscopy, SEM and optical microscopy. This work demonstrated the formation of structured domains, non-existent in films assembled from low anisotropic volume fractions or from high AVF, but without equilibration. Highly structured, low pitch films formed from the denser liquid crystalline fraction of the CNC suspension. Large domains were sandwiched between the top-disordered and bottom-ordered segments formed from merging tactoids near the isotropic/anisotropic interface during the EISA. In contrast, the non-equilibrated suspensions formed films that lacked the full colour-generating capacity and that had wider UV-Vis reflection spectra. These results highlight the importance of a long enough time window between the critical concentration and gelation stages, to develop tactoids and long-range order. The fact that equilibration had no or very little effect on suspensions that were fully isotropic prior to drying highlights the importance of equilibration at high AVF.

This thesis explored the restrictions and requirements that need to be considered in order to produce CNC solid structures that benefit from long-range helical order, such as impact resistant materials or colourful coatings on everyday materials.

REFERENCES

1. Hamad, W. *Photonic and Semiconductor Materials Based on Cellulose Nanocrystals;* Springer: 2016, pp 42.

2. Mehdi, J.; Foster, J. E. Recent advances in nanocellulose for biomedical applications. *Journal of Applied Polymer Science* **2015***, 132*, 1-19.

3. Valentini, L.; Bittolo Bon, S.; Fortunati, E.; Kenny, J. M. Preparation of transparent and conductive cellulose nanocrystals/graphene nanoplatelets films. *Journal of Materials Science* **2014***, 49*, 1009-1013.

4. Revol, J.; Bradford, H.; Giasson, J.; Marchessault, R. H.; Gray, D. G. Helicoidal self-ordering of cellulose microfibrils in aqueous suspension. *International Journal of Biological Macromolecules* **1992***, 14*, 170-172.

5. Beck, S.; Bouchard, J.; Chauve, G.; Berry, R. Controlled production of patterns in iridescent solid films of cellulose nanocrystals. *Cellulose* **2013***, 20*, 1401-1411.

6. Dumanli, A. G.; Kamita, G.; Landman, J.; van der Kooij, H.; Glover, B. J.; Baumberg, J. J.; Steiner, U.; Vignolini, S. Controlled, Bio-inspired Self-Assembly of Cellulose-Based Chiral Reflectors. *Advanced Optical Materials* **2014***, 2*, 646-650.

7. Ličen, M.; Majaron, B.; Noh, J.; Schütz, C.; Bergström, L.; Lagerwall, J.; Drevenšek-Olenik, I. Correlation between structural properties and iridescent colors of cellulose nanocrystalline films. *Cellulose* **2016***, 23*, 3601-3609.

8. Dumanli, A. G.; van der Kooij, Hanne M.; Kamita, G.; Reisner, E.; Baumberg, J. J.; Steiner, U.; Vignolini, S. Digital Color in Cellulose Nanocrystal Films. *ACS Applied Materials & Interfaces* **2014***, 6*, 12302-12306.

9. Mu, X.; Gray, D. G. Formation of Chiral Nematic Films from Cellulose Nanocrystal Suspensions Is a Two-Stage Process. *Langmuir* **2014***, 30*, 9256-9260.

10. Tardy, B. L.; Ago, M.; Guo, J.; Borghei, M.; Kämäräinen, T.; Rojas, O. J. Optical properties of self-assembled cellulose nanocrystals films suspended at planar–symmetrical interfaces. *Small* **2017***, 13,* 1-10.

11. Tran, A.; Hamad, W. Y.; MacLachlan, M. J. Tactoid Annealing Improves Order in Self-Assembled Cellulose Nanocrystal Films with Chiral Nematic Structures. *Langmuir* **2017**.

12. Wilts, B. D.; Whitney, H. M.; Glover, B. J.; Steiner, U.; Vignolini, S. Natural Helicoidal Structures: Morphology, Self-assembly and Optical Properties. *Materials Today: Proceedings* **2014***, 1*, 177-185.

13. Honorato-Rios, C.; Kuhnhold, A.; Bruckner, J. R.; Dannert, R.; Schilling, T.; Lagerwall, J. P. F. Equilibrium Liquid Crystal Phase Diagrams and Detection of Kinetic Arrest in Cellulose Nanocrystal Suspensions. *Frontiers in Materials* **2016***, 3*, 1-13.

14. Park, J. H.; Noh, J.; Schutz, C.; Salazar-Alvarez, G.; Scalia, G.; Bergstrom, L.; Lagerwall, J. P. F. Macroscopic Control of Helix Orientation in Films Dried from Cholesteric Liquid-Crystalline Cellulose Nanocrystal Suspensions. *ChemPhysChem* **2014**, *15*, 1477-1484.

15. Pan, J.; Hamad, W. Y.; Straus, S. K. Parameters Affecting the Chiral Nematic Phase of Nanocrystalline Cellulose Films. *Macromolecules* **2010**, *43*, 3851-3858.

16. Nguyen, T.; Hamad, W. Y.; MacLachlan, M. J. Tuning the iridescence of chiral nematic cellulose nanocrystals and mesoporous silica films by substrate variation. *Chemical Communications* **2013**, *49*, 11296-11298.

17. Gençer, A.; Schütz, C.; Thielemans, W. Influence of the Particle Concentration and Marangoni Flow on the Formation of Cellulose Nanocrystal Films. *Langmuir* **2017**, *33*, 228-234.

18. Shopsowitz, K.; Qi, H.; Hamad, W.; MacLachlan, M. Free-Standing Mesoporous Silica Films With Tunable Chiral Nematic Structures. *Nature* **2010**, *468*, 422-5.

19. Zhang, Y. P.; Chodavarapu, V. P.; Kirk, A. G.; Andrews, M. P. Nanocrystalline cellulose for covert optical encryption. *Journal of Nanophotonics* **2012**, *6*, 1-9.

20. Zhang, Y. P.; Chodavarapu, V. P.; Kirk, A. G.; Andrews, M. P. Structured color humidity indicator from reversible pitch tuning in self-assembled nanocrystalline cellulose films. *Sensors and Actuators B: Chemical* **2013**, 692-697.

21. Wenzlik, D.; Varanytsia, A.; Munoz, A.; Kosa, T.; Zentel, R.; Palffy-Muhoray, P. Distributed feedback lasing in cellulose films. *Optical Materials Express* **2014**, *4*, 162-171.

22. Bardet, R.; Roussel, F.; Coindeau, S.; Belgacem, N.; Bras, J. Engineered pigments based on iridescent cellulose nanocrystal films. *Carbohydrate Polymers* **2015**, *122*, 367-375.

23. Wang, B.; Walther, A. Self-Assembled, Iridescent, Crustacean-Mimetic Nanocomposites with Tailored Periodicity and Layered Cuticular Structure. *ACS Nano* **2015**, *9*, 10637-10646.

24. Bardet, R.; Belgacem, N.; Bras, J. Flexibility and Color Monitoring of Cellulose Nanocrystal Iridescent Solid Films Using Anionic or Neutral Polymers. *ACS Applied Materials & Interfaces* **2015**, *7*, 4010-4018.

25. Gu, M.; Jiang, C.; Liu, D.; Prempeh, N.; Smalyukh, I. I. Cellulose Nanocrystal/Poly(ethylene glycol) Composite as an Iridescent Coating on Polymer Substrates: Structure-Color and Interface Adhesion. *ACS Applied Materials & Interfaces* **2016**, *8*, 32565-32573.

26. Guidetti, G.; Atifi, S.; Vignolini, S.; Hamad, W. Y. Flexible Photonic Cellulose Nanocrystal Films. *Advanced Materials* **2016**, *28*, 10042-10047.

27. Reid, M. S.; Villalobos, M.; Cranston, E. D. Benchmarking Cellulose Nanocrystals: From the Laboratory to Industrial Production. *Langmuir* **2017**, *33*, 1583-1598.

28. Rånby, B. G. Aqueous Colloidal Solutions of Cellulose Micelles. *Acta chemica scandinavica* **1949**, *3*, 649-650.

29. Min Dong, X.; Revol, J.; Gray, G. D. Effect of microcrystallite preparation conditions on the formation of colloid crystals of cellulose. *Cellulose* **1998***, 5*, 19-32.

30. Hu, Z.; Cranston, E. D.; Ng, R.; Pelton, R. Tuning Cellulose Nanocrystal Gelation with Polysaccharides and Surfactants. *Langmuir* **2014***, 30*, 2684-2692.

31. Capron, I.; Rojas, O. J.; Bordes, R. **Behavior of nanocelluloses at interfaces**. *Current Opinion in Colloid & Interface Science* **2017***, 29*, 83-95.

32. Kinoshita, S. *Structutal colors in the realm of nature;* World scientific: 2008.

33. Apichattrabrut, T.; Ravi-Chandar, K. Helicoidal Composites. *Mechanics of Advanced Materials and Structures* **2006***, 13*, 61-76.

34. Kinoshita, S.; Yoshioka, S.; Miyazaki, J. Physics of structural colors. *Reports on Progress in Physics* **2008***, 71*, 1-30.

35. de Vries, H. Rotatory Power and other Optical Properties of Certain Liquid Crystals. *Acta Crystallographica* **1951***, 4*, 219-226.

36. Dong, X. M.; Kimura, T.; Revol, J.; Gray, D. G. Effects of Ionic Strength on the Isotropic-Chiral Nematic Phase Transition of Suspensions of Cellulose Crystallites. *Langmuir* **1996***, 12*, 2076-2082.

37. de Gennes, P. G.; Prost, J. The physics of liquid crystals. In International series on monographs on physics No 83: 1993.

38. Straley, J. P. Theory of piezoelectricity in nematic liquid crystals, and of the cholesteric ordering. *Physical review A* **1976***, 14*, 1835-1841.

39. Orts, W. J.; Godbout, L.; Marchessault, R. H.; Revol, J. Enhanced Ordering of Liquid Crystalline Suspensions of Cellulose Microfibrils: A Small Angle Neutron Scattering Study. *Macromolecules* **1998***, 31*, 5717-5725.

40. Araki, J.; Kuga, S. Effect of Trace Electrolyte on Liquid Crystal Type of Cellulose Microcrystals. *Langmuir* **2001***, 17*, 4493-4496.

41. Habibi, Y.; Lucia, L. A.; Rojas, O. J. Cellulose Nanocrystals: Chemistry, Self-Assembly, and Applications. *Chemical Reviews* **2010***, 110*, 3479-3500.

42. Jativa, F.; Schutz, C.; Bergstrom, L.; Zhang, X.; Wicklein, B. Confined self-assembly of cellulose nanocrystals in a shrinking droplet. *Soft Matter* **2015***, 11*, 5374-5380.

43. Onsager, L. The effects of shape on the interactions of colloidal particles. *Annals New York Academy of Sciences* **1949***, 51*, 627-659.

44. Revol, J.; Marchessault, R. H. In vifro chiral nematic ordering of chitin crystallites. *International Journal of Biological Macromolecules* **1993***, 15*, 329-335.

45. Marchessault, R. H.; Morehead, F. F.; Walter, N. M. Liquid Crystal Systems from Fibrillar Polysaccharides. *Nature* **1959**, 632-633.

46. Beck-Candanedo, S.; Roman, M.; Gray, G. D. Effect of Reaction Conditions on the Properties and Behavior of Wood Cellulose Nanocrystal Suspensions. *Biomacromolecules* **2005***, 6*, 1048-1054.

47. Chen, Q.; Liu, P.; Nan, F.; Zhou, L.; Zhang, J. Tuning the Iridescence of Chiral Nematic Cellulose Nanocrystal Films with a Vacuum-Assisted Self-Assembly Technique. *Biomacromolecules* **2014***, 15*, 4343-4350.

48. Liu, D.; Wang, S.; Ma, Z.; Tian, D.; Gu, M.; Lin, F. Structure-color mechanism of iridescent cellulose nanocrystal films. *RSC Advances* **2014***, 4*, 39322-39331.

49. Beck, S.; Bouchard, J.; Berry, R. Controlling the Reflection Wavelength of Iridescent Solid Films of Nanocrystalline Cellulose. *Biomacromolecules* **2011***, 12*, 167-172.

50. Agarwal, U. Tailoring the yield and characteristics of wood cellulose nanocrystals (CNC) using concentrated acid hydrolysis. *Cellulose* **2015***, 22*, 1753-1762.

51. Abitbol, T.; Kam, D.; Levi-Kalisman, Y.; Gray, D. G.; Shoseyov, O. Surface Charge Influence on the Phase Separation and Viscosity of Cellulose Nanocrystals. *Langmuir* **2018***, 34*, 3925-3933.

52. Hirai, A.; Inui, O.; Horii, F.; Tsuji, M. Phase Separation Behavior in Aqueous Suspensions of Bacterial Cellulose Nanocrystals Prepared by Sulfuric Acid Treatment. *Langmuir* **2009***, 25*, 497-502.

53. Gray, G. D.; Min Dong, X. Effect of Counterions on Ordered Phase Formation in Suspensions of Charged Rodlike Cellulose Crystallites. *Langmuir* **1997***, 13*, 2404-2409.

54. Bruckner, J. R.; Kuhnhold, A.; Honorato-Rios, C. Enhancing Self-Assembly in Cellulose Nanocrystal Suspensions Using High-Permittivity Solvents. *Langmuir* **2016***, 32*, 9854-9862.

55. Lagerwall, J. P. F.; Schütz, C.; Salajkova, M.; Park, J. H.; Scalia, G.; Bergstrom, L. Cellulose nanocrystal-based materials: from liquid crystal self-assembly and glass formation to multifunctional thin films. *NPG Asia Materials* **2014***, 6*, 1-12.

56. Shafiei-Sabet, S.; Hamad, W. Y.; Hatzikiriakos, S. G. Rheology of Nanocrystalline Cellulose Aqueous Suspensions. *Langmuir* **2012***, 28*, 17124-17133.

57. Wang, P.; Hamad, W. Y.; MacLachlan, M. J. Structure and transformation of tactoids in cellulose nanocrystal suspensions. *Nature Communications* **2016***, 7*, 1-7.

58. Gray, G. D.; Mu, X. Chiral Nematic Structure of Cellulose Nanocrystal Suspensions and Films; Polarized Light and Atomic Force Microscopy. *Materials* **2015***, 8*, 7873-7888.

59. Klemm, D.; Philipp, B.; Heinze, T.; Heinze, U.; Wagenknecht, W. General Considerations on Structure and Reactivity of Cellulose: Section 2.1-2.1.4. In *Comprehensive Cellulose Chemistry*Wiley-VCH Verlag GmbH & Co. KGaA: 2004; pp 9-29.

60. Tang, H.; Guo, B.; Jiang, H.; Xue, L.; Li, B.; Cao, X.; Zhang, Q.; Li, P. Fabrication and characterization of nanocrystalline cellulose films prepared under vacuum conditions. *Cellulose* **2013***, 20*, 2667-2674.

61. Deegan, R. D.; Bakajin, O.; Dupont, T. F.; Huber, G.; Nagel, S. R.; Witten, T. A. Capillary flow as the cause of ring stains from dried liquid drops. *Nature* **1997***, 389*, 827-829.

62. Mu, X.; Gray, D. G. Droplets of cellulose nanocrystal suspensions on drying give iridescent 3-D ‘‘coffee-stain’’ rings. *Cellulose* **2015***, 22*, 1103-1107.

63. Gray, D. G.; Mu, X. Twist–Bend Stage in the Relaxation of Sheared Chiral Nematic Suspensions of Cellulose Nanocrystals. *ACS Omega* **2016***, 1*, 212-219.

64. Hoeger, I.; Rojas, O. J.; Efimenko, K.; Velev, O. D.; Kelley, S. S. Ultrathin film coatings of aligned cellulose nanocrystals from a convective-shear assembly system and their surface mechanical properties. *Soft Matter* **2011***, 7*, 1957-1967.

65. Wang, B.; Walther, A. Self-Assembled, Iridescent, Crustacean-Mimetic Nanocomposites with Tailored Periodicity and Layered Cuticular Structure. *ACS Nano* **2015***, 9*, 10637-10646.

66. Schlesinger, M.; Hamad, W. Y.; MacLachlan, M. J. Optically tunable chiral nematic mesoporous cellulose films. *Soft Matter* **2015***, 11*, 4686-4694.

67. Fu, T.; Montes, F.; Suraneni, P.; Youngblood, J.; Weiss, J. The Influence of Cellulose Nanocrystals on the Hydration and Flexural Strength of Portland Cement Pastes. *Polymers* **2017***, 9*, 1-16.

68. Semenikhin, N. S.; Kadasala, N. R.; Moon, R. J.; Perry, J. W.; Sandhage, K. H. Individually Dispersed Gold Nanoshell-Bearing Cellulose Nanocrystals with Tailorable Plasmon Resonance. *Langmuir* **2018***, 34*, 4427-4436.

69. Du, L.; Zhong, T.; Wolcott, M. P.; Zhang, Y.; Qi, C.; Zhao, B.; Wang, J.; Yu, Z. Dispersing and stabilizing cellulose nanoparticles in acrylic resin dispersions with unreduced transparency and changed rheological property. *Cellulose* **2018***, 25*, 2435-2450.

70. Majoinen, J.; Kontturi, E.; Ikkala, O.; Gray, D. G. SEM imaging of chiral nematic films cast from cellulose nanocrystal suspensions. *Cellulose* **2012***, 19*, 1599-1605.

71. Petersen, C.; Heldmann, C.; Johannsmann, D. Internal Stresses during Film Formation of Polymer Latices. *Langmuir* **1999***, 15*, 7745-7751.

72. Francis, L. F.; Mccormick, A. V.; Vaessen, D. M.; Payne, J. A. Development and measurement of stress in polymer coatings. *Journal of Materials Science* **2002***, 37*, 4717-4731.

73. Natarajan, B.; Emiroglu, C.; Obrzut, J.; Fox, D. M.; Pazmino, B.; Douglas, J. F.; Gilman, J. W. Dielectric Characterization of Confined Water in Chiral Cellulose Nanocrystal Films. *ACS Applied Materials & Interfaces* **2017***, 9*, 14222-14231.

74. Bodiguel, H.; Leng, J. Imaging the drying of a colloidal suspension. *Soft Matter* **2010***, 6*, 5451-5460.

75. Chen, W.; Gray, D. G. Interfacial Tension between Isotropic and Anisotropic Phases of a Suspension of Rodlike Particles. *Langmuir* **2002***, 18*, 633-637.

APPENDIX 1

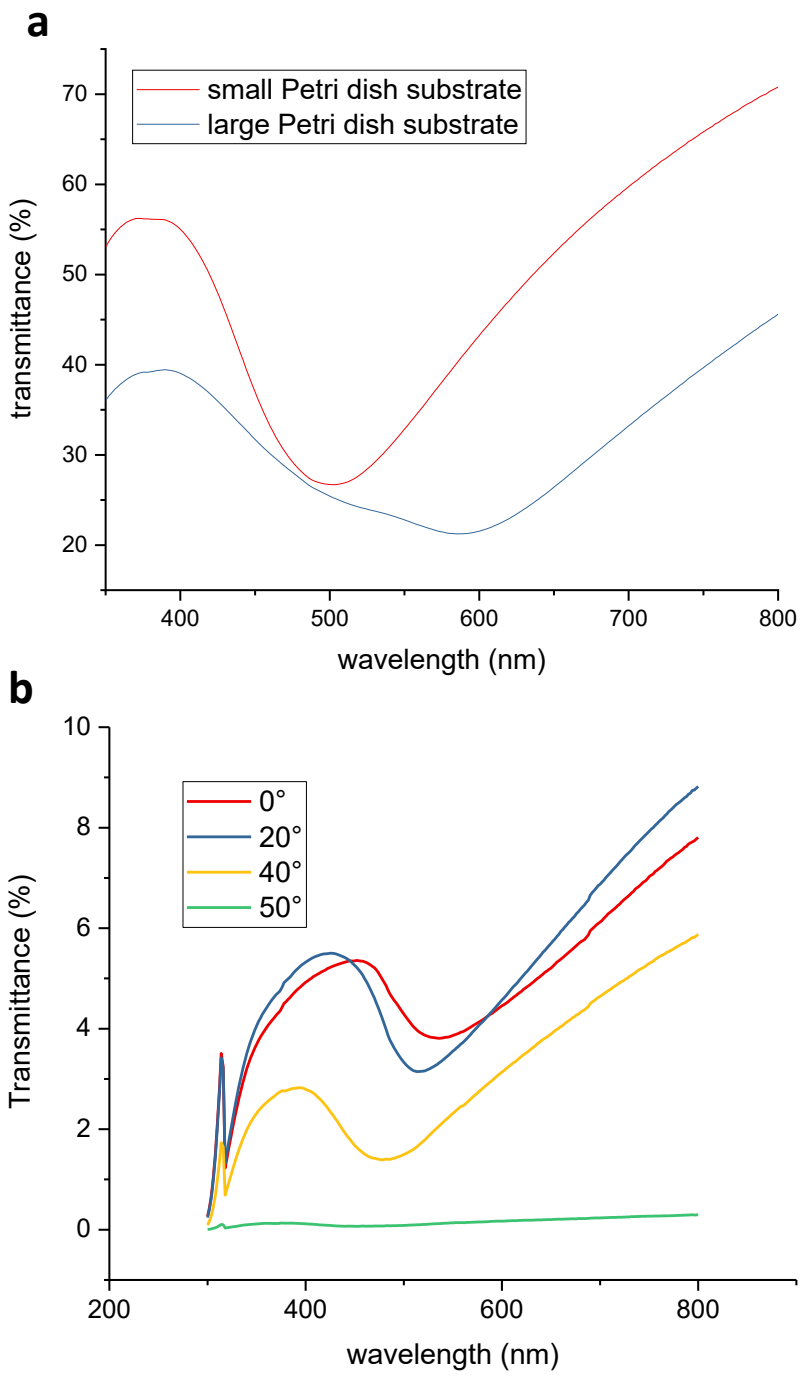

Appendix 1. (a) Transmission spectra of films dried in a small 3,5 cm Petri dish and a large 5,5 cm Petri dish. The transmission spectral bandwidth is wider for the film dried in a large Petri dish, which could result from a wider distribution of pitch sizes within the film, and therefore poorer helical ordering. (b) Transmission spectra at various incidence angles for the incoming beam. This iridescence phenomenon arises according to Equation 1, which states that the incidence angle influences the reflected light.

APPENDIX 2

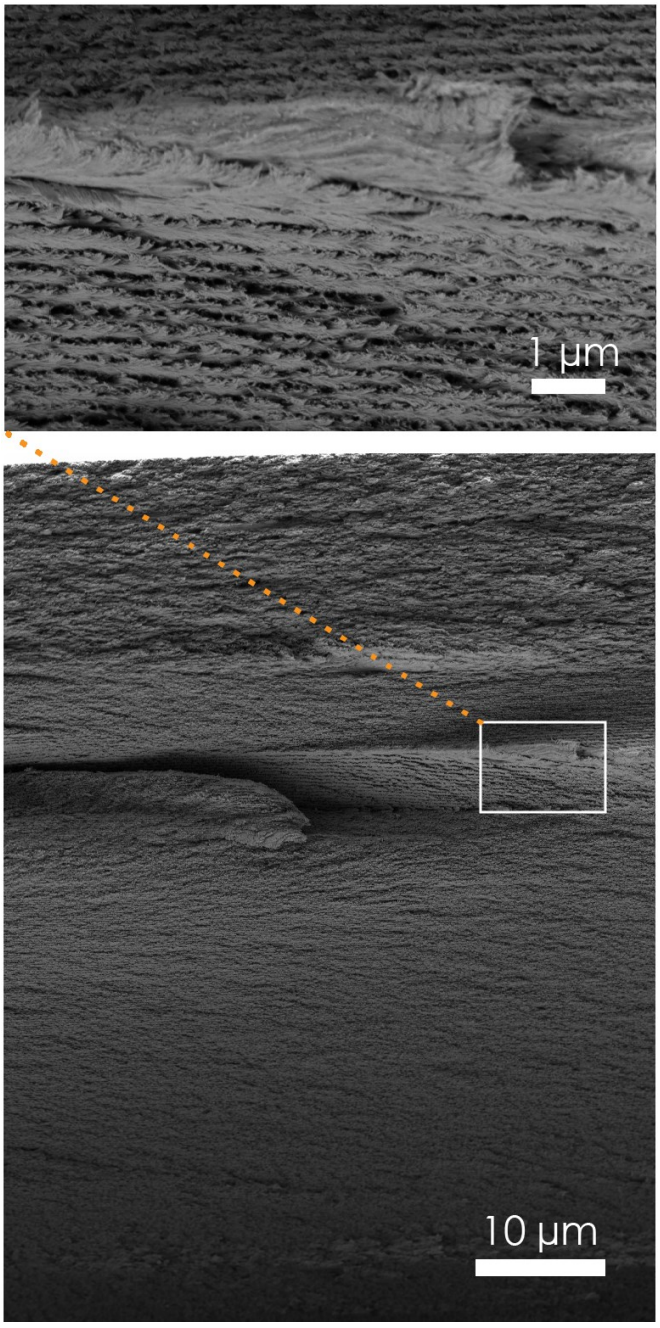

Appendix 2. The lower SEM image is a cross-section, through the thickness, of the E_w6 sample film, fractured and image at the radial centre. The upper image is zoomed in from the white box in the lower image. This figure conveys that the chiral nematic domain, which was zoomed, is protruding from the cross-section due to its elliptical nature, and the chiral nematic ordering within the domain is sound. The fracture passed around the domain rather than going through it, since the high level of helical order within the domain prevents fracture propagation.